# Reporting of methods for automated devices: A systematic review and recommendation for studies using FlowCam for phytoplankton

**Article** *in* Limnology and Oceanography, Methods · June 2022

DOI: 10.1002/lom3.10496

CITATIONS
0

READS
92

**5 authors**, including:

Bianca Owen
Murdoch University
**1** PUBLICATION **0** CITATIONS
SEE PROFILE

James Tweedley
Murdoch University
**144** PUBLICATIONS **1,813** CITATIONS
SEE PROFILE

LIMNOLOGY and OCEANOGRAPHY: METHODS

ASLO

*Limnol. Oceanogr.: Methods* 2022

doi: 10.1002/lom3.10496

# Reporting of methods for automated devices: A systematic review and recommendation for studies using FlowCam for phytoplankton

**Bianca M. Owen** [1,2,3]* **Chris S. Hallett** [1] **Jeffrey J. Cosgrove,** [4] **James R. Tweedley** [1,3] **Navid R. Moheimani** [2,3]

[1]Centre for Sustainable Aquatic Ecosystems, Harry Butler Institute, Murdoch University, Murdoch, Western Australia, Australia
[2]Algae Research and Development Centre, Murdoch University, Murdoch, Western Australia, Australia
[3]College of Science, Health, Engineering and Education, Murdoch University, Murdoch, Western Australia, Australia
[4]Department of Biodiversity Conservation and Attractions, Kensington, Western Australia, Australia

## *Abstract*

Accurate and detailed reporting of methods is essential for scientific progress, yet it is widely accepted that authors across all scientific fields tend to provide insufficient methods detail. Given the recent proliferation of automated and semi-automated technologies for data collection, to address this widespread issue the details needed for interpretation and reproducibility for each specific technique first need to be identified. A systematic literature review assessed the comprehensiveness of method details reported by 116 peer-reviewed studies published between 2017 and 2020 using the FlowCam (a widely used imaging flow cytometer) to image phytoplankton, finding all to be lacking in critical details, inhibiting reproducibility, and limiting the veracity of some findings. Through this review and three case studies, we identify several key method details that should be reported by FlowCam studies to ensure their findings are credible, comparable, and replicable and illustrate the wide-reaching implications for not doing so. Future studies using FlowCam for phytoplankton analyses should ensure clear reporting of all relevant details relating to the FlowCam unit, sample preparation, run settings, post-processing of images, and the considered use of only verified measurement outputs. A methods reporting template is presented as a guideline intended to enhance the quality, interpretability, and repeatability of future FlowCam papers. The pervasiveness of inadequacies in FlowCam methods reporting identified here highlights how vital it is for users of any automated or semi-automated scientific technologies to have a clear understanding of the impact of all method details on their findings, and to report these details adequately.

It is generally understood that the methods section of a paper should not only provide the reader with an understanding of how a study was conducted, but also sufficient detail to allow for the independent replication of research findings. Despite this, it is widely acknowledged that most published studies lack sufficient method details and science is suffering from a pervasive reproducibility problem (Baker 2016; Munafò et al. 2017; Marqués et al. 2020). Over the past two decades, there has been an increasing reliance on automated or semi-automated data collection technologies with a recent rapid proliferation of commercially available automated devices designed for a multitude of specific tasks (Keitt and Abelson 2021). The outcomes of studies using such automated devices will depend on numerous, highly detailed aspects of hardware and software configurations and methods employed, particularly when compared to traditional techniques with long-standing widely accepted protocols (Aaron and Chew 2021). As modern devices become more "user-friendly," their intricate functioning becomes more opaque as important methods parameters can be changed by the click of a mouse, leading researchers to be unclear on which details can influence data and subsequent conclusions and are therefore salient to report (Heddleston et al. 2021). Failure to report seemingly inconsequential method details in such cases can have surprising flow-on effects on study findings and lead to confusing contradictory conclusions between studies (Aaron and Chew 2021).

Specific standardized reporting guidelines that identify and detail the necessary methods to be reported for each individual technology are needed to address widespread reporting inadequacies, as the intricacies of each emerging technique

*Correspondence: b.owen@murdoch.edu.au

Additional Supporting Information may be found in the online version of this article.

prevent a single prescription across all devices (Munafò et al. 2017). In human health research, the importance of specific reporting guidelines is well established with an online library (equator-network.org) of over 500 searchable reporting guidelines and numerous studies quantifying the improvements to study reproducibility when such guidelines are followed (Plint et al. 2006; Kane et al. 2007; Turner et al. 2012). Detailed methods reporting guidelines have also been developed in part or in full for a range of specific aquatic technologies, for example, in vivo chlorophyll fluorescence (Cosgrove and Borowitzka 2006, 2010), aquatic environmental DNA (Goldberg et al. 2016), and aquatic microplastic quantification (Vandermeersch et al. 2015).

Monitoring of phytoplankton communities is important across industry, research, and natural resource management and is mandated under wide-reaching legislation including the US Clean Water Act and EU Water Framework Directive (Borja et al. 2008; Hallett et al. 2016). Historically, phytoplankton analysis has relied on manual microscopy-based identification and enumeration of each individual cell by highly trained taxonomists, a well-established technique, with standardized methods dating back more than a hundred years (Kofoid 1897; Langelier 1928; Soares et al. 2011). Over the past two decades, with decreased hardware costs and increasingly sophisticated image analysis software, a wide range of technologies specifically for digital imaging of plankton and the subsequent manual, semi-automated, or automated classification of those images have become available and are being applied to measure and monitor plankton in aquatic systems (Benfield et al. 2007; Sun and Sun 2014). These technologies reportedly allow for decreased sample turnaround time and increased sampling frequency, sample numbers, and/or volumes, while also adding data types and plankton types that are impossible or prohibitively time-consuming to collect with traditional microscopy (Beutler 2003; Babin et al. 2005; Sieracki et al. 2010). They have been relied on more heavily during the COVID-19 pandemic, allowing laboratories to continue their monitoring commitments with taxonomists working remotely (Clayton et al. 2022). These devices can rapidly and easily produce huge datasets, but before using them for monitoring and research it is important that we can identify that their outputs are accurate, reliable, and well-understood, especially when comparing findings to previous studies, incorporating them into existing long-term datasets or using them to inform critical decisions on when to close or reopen waterbodies to human use or consumption (Zingone et al. 2015; Wasmund et al. 2017). In addition, as artificial intelligence algorithms improve there is a growing demand for shared plankton image datasets, but the inclusion criteria for global open-access data repositories require clear, detailed device-specific methods reporting (Neeley et al. 2021).

The FlowCam (Yokogawa Fluid Imaging Technologies) is a commercially available imaging flow cytometer which has been used to image phytoplankton for a wide range of purposes since 1998, yet no uniform system exists for reporting its use in research applications. This is problematic, as it allows for wide variety in the level of method detail reported by different studies, which may be inadequate to ensure that methods can be reliably understood, were appropriate and can be reproduced. Using the FlowCam as an example, we aim to highlight the importance of detailed reporting of methods by studies using emerging technologies. We systematically review the methods-reporting of peer-reviewed studies published over four years (2017–2020) using FlowCam to analyze phytoplankton, and identify the key method details and choices that can impact findings with the support of three case studies. We propose a series of clear reporting guidelines for researchers that would allow them to present detailed, reproducible methods for future FlowCam studies, which may serve as an example for how to address widespread methods reporting inadequacies, one technique at a time.

## The FlowCam for plankton analysis

The FlowCam is an automated particle analysis system that uses a combined microscope, digital camera, and flow cytometer to digitally image, count, and measure microorganisms. Water samples are collected and fed into the device, which pumps them through a *flow cell* held in front of a microscope lens coupled with a digital camera. Depending on the combination of microscope objective and flow cell, the FlowCam can image particles from 1 $\mu$m to 2 mm in size. Images can be captured in three different modes; *auto-image* mode (imaging at timed intervals), *scatter-triggered* mode (imaging when particles are detected), and *fluorescence-triggered* mode (imaging when fluorescent particles are detected). The associated *VisualSpreadsheet* software is used to control the FlowCam and run samples, capture and crop images, extract particle parameters for each cropped image, and as a user interface for viewing and sorting these images. The FlowCam with this software (and the optional software add-on, *Classifier Advanced*) is also advertised for its ability to semi-automatically classify collected images using user-defined *image libraries* and statistical pattern-recognition algorithms (Yokogawa Fluid Imaging Technologies 2021).

FlowCam exhibits many purported advantages over traditional microscopic observation of plankton; providing a permanent digital record of samples, rapidly collecting multiple measurements of cells and, when using the auto-classification capabilities, decreased time and labor requirements for identifying cells (Sieracki et al. 1998; Spaulding et al. 2012; Álvarez et al. 2014). This equipment has now been used to provide phytoplankton monitoring data around the world, including Spain, the Philippines, the United States, and Brazil (See et al. 2005; Sieracki et al. 2010; Álvarez et al. 2012; Camoying and Yñiguez 2016). FlowCam has been used in the identification and quantification of harmful algal bloom species (Buskey and Hyatt 2006; Lehman et al. 2013), detailed investigations of zooplankton and phytoplankton interactions (Ide

et al. 2008), and studies of the broad seasonal variations in abundance, size structure, and diversity of plankton communities (Álvarez et al. 2011, 2014; Camoying 2016).

## Issues with reporting of methods among FlowCam studies

A systematic literature review (Moher et al. 2010; Okoli and Schabram 2010) was conducted to critically assess and compare methods reporting in recent papers using FlowCam to image phytoplankton. Peer-reviewed journal articles using the FlowCam to image phytoplankton published between 2017 and 2020 were included to identify key methods reporting issues and develop reporting recommendations for what should now be an established technique. As search results vary by database (Calver et al. 2017), a separate search was conducted for the term "FlowCam" searching within "all fields" of articles and review papers published between 01 January 2017 and 31 December 2020 in both Scopus and Web of Science Core Collection (accessed 28 June 2021). All aquatic FlowCam studies compiled by Yokogawa Fluid Imaging Technologies on their website (https://info.fluidimaging.com/hubfs/documents/Aquatics%20Publications/Aquatic%20Papers%20List.pdf, accessed 28 June 2021) were also considered. The three sources, respectively, yielded 177, 80, and 128 results, reduced to 185 total studies after duplicates were removed. Each of these 185 studies was manually checked for the four inclusion criteria; (i) the study was published in a peer-reviewed journal, (ii) the study was available in English, (iii) the study was published between 01 January 2017 and 31 December 2020, and (iv) the study used a FlowCam to image phytoplankton for any reason. The resulting 116 studies meeting these criteria were reviewed, with their reported FlowCam method details summarized in Table 1.

The descriptions of FlowCam methods among the 116 papers reviewed generally lack detail, with 3% of studies simply stating that they used a "FlowCam" to collect data, with no further description of how this was achieved (Arrigo et al. 2017; Giling et al. 2017; Noh et al. 2018; Poulin et al. 2018*a*, see Table 1). Given that there are numerous user choices when operating the FlowCam (e.g., objective and flow cell size, image collection mode, etc.), providing limited or no context on the way it was used presents significant barriers to critically understanding how the results were obtained and removes the capacity for reproducibility.

Published FlowCam studies differed markedly in the detail of reported methods (Table 2), making comparisons between studies challenging. This lack of consistent and detailed description hinders the reproducibility of published methods and thus confidence in the accuracy of findings. In addition, new users or those considering the purchase of a FlowCam unit are left uninformed as to what they can realistically expect from the device and the amount of rigor required to achieve meaningful outputs. These issues are not only restricted to the FlowCam, nor even to digital imaging technologies in general, but are relevant to many other techniques and devices in the current age of increased automation and reduced reliance upon manual methods (Munafò et al. 2017; Marqués et al. 2020). For the FlowCam specifically, five key gaps in the current reporting of published methods have been identified: (i) FlowCam unit technical specifications, (ii) sample type and preparation, (iii) FlowCam processing details, (iv) post-processing of images, and (v) the use of FlowCam outputs. Each is now critically evaluated in more detail.

### FlowCam unit technical specifications

As the FlowCam is a relatively expensive piece of equipment (approximately US$112,000 for FlowCam 8400-C [pers. comm., S. Rembold, Kenelec Scientific]), a relatively small number of machines have been produced (1000 units as of December 2020). Eleven different FlowCam models suitable for phytoplankton analysis have been released since the FlowCam was first produced in 1998 and the specifications of individual units vary considerably both between and within models. When purchasing a new FlowCam, many options are available in terms of digital camera, cell size range, image capture modes, fluid movement mechanisms, and other features (Table 3). Due to the cost of machines, older FlowCam models are likely to be retained for extended periods in research institutions (some of the earliest B2 units are still being used in recent years, see Table 1), and Yokogawa Fluid Imaging Technologies provides the option for existing FlowCam units to be upgraded to have newer features.

Given that each individual FlowCam unit has a unique set of technical specifications regardless of model number, it is important that these details are accurately presented by studies employing a FlowCam. It is apparent that the variability present between individual FlowCam units and the implications of those variances are not well recognized by many users, as many studies do not report which FlowCam model was used (53%), and the vast majority of studies do not provide any further detail about its specifications (85%). Claims about the efficiency and capabilities of FlowCam analyses will be extremely unit-dependent. However, studies continue to make generalized conclusions about the time-efficiency of "FlowCam" analysis since the 2016 release of the more efficient 8000-series models, without stating which FlowCam model they used (Kydd et al. 2018). Conclusions regarding the quality of images or image-based outputs/measurements from the FlowCam are similarly problematic when the FlowCam unit details are not stated (e.g., "images smaller than 50 $\mu$m are difficult to identify as detritus or cells"; Lin et al. 2019). Digital camera specifications directly impact image quality and as a result, the accuracy of taxonomic identifications (Bayer et al. 2001), yet only 2% of studies stated their unit's camera resolution (increased resolution can capture more key identifiable features) and only 9% stated whether their unit was equipped with a color or monochrome camera (color

**Table 1.** Reported details of methods used in all 116 peer-reviewed studies published between 2017 and 2020 that used FlowCam to image phytoplankton, sorted by publication date (most recent first). Dashses (—) denote omitted method details.

| Reference | FlowCam used for | FlowCam model | VS version | Sample composition | Sample preservation | Sample pre-filtration | Sample concentration or dilution | FlowCam processing mode | Flow cell, objective lens | FlowCam processing details | Image sorting method |
|---|---|---|---|---|---|---|---|---|---|---|---|
| | ID, abundance, size (outputs used) | Model details, camera, pump | Version number | Mixed/ monoculture | Fresh/preservative used | Size ranges specified | Concentration specified | Auto-image, scatter-trigger, fluoro-trigger (wavelength) | FC/FOV (flow cell size) objective | Sample volume (mL) (imaged/ processed), number imaged per sample (particles), flow rate (mL $min^{-1}$), run time (min), image capture frame rate (FPS) | Auto/manual, with VS/external |
| Martínez et al. (2020) | ID, abundance | VS-4, 5-mL syringe pump | 4.2.52 | Mixed | Lugol's solution | 55–300 $\mu$m | Diluted to < 600 cells $mL^{-1}$ | Auto-image | (–) 300 4× | 1500 particles, 1.7 mL $min^{-1}$, 20 FPS | Auto with VS and external software, then manual |
| Martin et al. (2020) | Size (ABD) | FlowCam 8000 | — | Monoculture | — | — | — | Auto-image | FOV50 20× | ≥ 5000 particles | — |
| Kuhlisch et al. (2020) | Abundance (via ABD) | IV | — | Monoculture | — | — | — | — | FC300 4× | 20 mL (–) | — |
| Kimambo et al. (2020) | ID, size (ABD, ESD) | Benchtop VS4 serial 5049 2012 | 3.0 | Mixed | Lugol's | — | — | Auto-image | FC100 10× | — | — |
| Jyothibabu et al. (2020) | ID*, abundance, size (ABD†) | — | 2.4 | Mixed | Fresh | 20–300 $\mu$m | Concentrated to ×10 | Fluoro-trigger (525 nm) | FOV300 4× | — | Manual with VS |
| Harvey et al. (2020) | ID, abundance, size (L, W) | — | — | Mixed | Formalin | < 200 $\mu$m | — | Auto-image | (–) 300 (–) | ~ 27,000 particles, 2 mL $min^{-1}$ | — |
| Chaffin et al. (2020*a*) | Abundance, size (ABD) | — | 4.0.27 | Mixed | Formalin | — | — | Auto-image | (–) 10× | 8000 particles | Auto with VS, then manual |
| Kerr et al. (2020) | ID, abundance | VS-IVc | 4.1.95 | Mixed | Fresh | < 63 $\mu$m | — | Auto-image | (–) 300 4× | 11,371 particles, 6–12 FPS | Manual with VS, auto with external |
| Walcutt et al. (2020) | Abundance‡,§, size (ESD)‡,§ | — | 3.2.3, 4.0.27 | 3 monocultures, mixed | Lugol's, formaldehyde | — | Diluted | Fluoro-trigger (–) | (–) 80 10×, (–) 300 10× | 0.1–0.15 mL $min^{-1}$, 0.04–1 FPS | (–) with VS |
| Rue et al. (2020) | ID, abundance | VS-IV | — | Mixed | Lugol's | < 100 $\mu$m | — | Auto-image | (–) 10× | 5 mL processed, 0.15 mL $min^{-1}$, 0.04–1 FPS | Auto with VS, then manual |
| Parra et al. (2020) | ID, abundance, size (SB) | — | — | Mixed | — | < 202 $\mu$m | None | Fluoro-trigger (–) | (–)100 10× | — | — |
| Greer et al. (2020) | ID, abundance, size (SB) | B3 benchtop series | — | Mixed | — | — | — | Trigger (–) | (–) 300 4× | 3 × 4.9 mL processed | Manual |
| Menden-Deuer et al. (2020) | Abundance*,‖,¶, size (ESD)*,‖,¶ | Benchtop B3 series | — | 8 monocultures, mixed | Fresh | None, 5–202 $\mu$m | None, concentrated to × 10 | Auto-image, fluoro-trigger (–) | FC50 20×, FC50 20×, FC100 10× | 3 × 0.3–5 mL processed, 3–10 min | Manual |

*(Continues)*

**Table 1.** Continued

| Reference | FlowCam used for | FlowCam model | VS version | Sample composition | Sample preservation | Sample pre-filtration | Sample concentration or dilution | FlowCam processing mode | Flow cell, objective lens | FlowCam processing details | Image sorting method |
|---|---|---|---|---|---|---|---|---|---|---|---|
| Wu et al. (2020*a*) | Abundance#, size (ABD, ESD)# | — | — | Mixed | Fresh | >40 $\mu$m, 40–100 $\mu$m, 100–300 $\mu$m | Concentrated | Auto-image | FC50 20×, FC100 10×, FC300 4× | 0.05–0.4 mL min$^{-1}$, 2–5 min, 2–20 FPS | — |
| Zamyadi et al. (2020) | Abundance | — | — | Monoculture | Fresh | — | — | — | (–) 20× | 2 mL (–), 0.025 mL/min, 20 FPS | — |
| Montes et al. (2020) | ID, abundance | — | — | Mixed | Glutaraldehyde | 40–100 $\mu$m | — | — | (–) 20× | 50 mL (–) | — |
| Chaffin et al. (2020*b*) | ID, size (–) | — | 4.0.27 | Mixed | — | — | — | Auto-image | (–) 20×, (–) 10×, (–) 4× | 8000 particles | Auto with VS, then manual |
| Reul et al. (2020) | Abundance, size (–) | Benchtop VS4C/488/DSP | — | Mixed | Fresh | >45 $\mu$m | Concentrated to ×100 | Auto-image | (–) 100 10× | — | Manual |
| Bartual et al. (2020) | ID, abundance, size (L, W, "diameter" [–]) | — | — | Mixed | Fresh, formaldehyde | 10–100 $\mu$m, 100–250 $\mu$m | Concentrated to ×40, ×100 | Auto-image | (–) 100 10×, (–) 300 4× | 100–125 mL processed | Auto with external |
| Farrow et al. (2020) | ID, abundance (via ABD) | VS-4 series | 3.4.5 | Mixed | Fresh | <100 $\mu$m | Diluted to ≤ 2 cells per frame | Fluoro-trigger (488 nm) | (–) 10× | 0.2 mL min$^{-1}$ | Auto with VS, then manual |
| Cornwell et al. (2020) | ID, abundance, size (ABD) | VS-IVc | 4.1.95 | Mixed | Lugol's | <100 $\mu$m | Concentrated to ×10 | Auto-image | (–) 100 10× | 25 mL (–), ~28,000 particles, 20 FPS | Manual with VS |
| Loria et al. (2020) | ID, abundance | Benchtop B3 Series | | Mixed | — | — | Concentrated | — | (–) 100 10× | 5 mL (–) | Manual |
| Krause and Lomas (2020) | Abundance, size (SB) | VS series benchtop | — | Mixed | Fresh | <200 $\mu$m | — | Auto-image | (–) 200 10× | 10 mL (–) | Manual |
| Casas-Monroy et al. (2020) | Abundance* | — | — | Mixed | Lugol's | 10–53 $\mu$m, 53–295 $\mu$m | Concentrated to ×40 | Auto-image | (–) 80 10×, (–) 300 4× | ~1 mL imaged, 10 and 60 min | Manual with VS |
| Karnan et al. (2020) | ID, abundance, size (ABD, AR)† | Portable VS4 | — | Mixed | — | 20–300 $\mu$m | Concentrated to ×10–50 | — | FOV300 4× | — | Auto (–) with VS |
| Lehman et al. (2020) | Size (–) | — | — | Mixed | Lugol's | <300 $\mu$m, >300 $\mu$m | — | — | (–) 10×, (–) 4× | — | — |
| Fung and Ackerman (2020) | ID, abundance | VS series | — | Mixed | — | <35 $\mu$m, 35–100 $\mu$m | Diluted to ≤ 2 cells per frame | Auto-image, fluoro-trigger (488 nm) | (–) 20×, (–) 10× | 1–3 mL (–), 0.05–0.2 mL min$^{-1}$, 20 FPS | Manual |
| Hozumi et al. (2020) | Abundance, size (ESD)# | — | — | Mixed | Lugol's | — | — | — | (–) 100 10× | ~0.2 mL processed | Manual |
| Tran and Ackerman (2019) | ID, abundance | Benchtop B3 VS4 series | 3.2 | Mixed | Preserved (–) | <35 $\mu$m | Diluted to × 0.5 | Fluoro-trigger (488, 650 nm) | (–) 50 20× | ~2900 particles, 0.05 mL min$^{-1}$ | Manual, then auto, then manual with VS |
| Tian-Tian et al. (2019) | Size (ESD) | 8000 series, 1920 × 1200 | — | Monoculture | — | — | — | — | (–) 10× | — | — |
| Hrycik et al. (2019) | ID*, abundance*, size (ABD*,†, SB) | Benchtop B3 series VS-IV | — | Mixed | Lugol's | 63–100 $\mu$m, 100–300 $\mu$m | Diluted to × 0.25, ~1 cell per frame | Auto-image | (–) 10×, (–) 4× | 1 mL processed | Manual with VS |
| Chaplin et al. (2019) | ID, abundance, size (L) | VS series benchtop | — | Mixed | Bouin's solution | — | — | Auto-image | (–) 200 10× | — | Manual |

*(Continues)*

**Table 1.** Continued

| Reference | FlowCam used for | FlowCam model | VS version | Sample composition | Sample preservation | Sample pre-filtration | Sample concentration or dilution | FlowCam processing mode | Flow cell, objective lens | FlowCam processing details | Image sorting method |
|---|---|---|---|---|---|---|---|---|---|---|---|
| Zhang et al. (2019) | ID, abundance, size (ESD) | — | — | Mixed | Formaldehyde | 77–300 $\mu$m, 300–600 $\mu$m | Diluted to × 0.125–0.25 | Auto-image | (–) 300 4×, (–) 600 4× | 5 mL (–), 20 min | — |
| Joy-Warren et al. (2019) | ID, abundance, size (GL, GT, L, W) | VS IVc | — | Mixed | — | > 300 $\mu$m | — | — | (–) 4× | — | Auto with external |
| Park et al. (2019*a*) | ID, abundance, size (–)* | 8100-C | — | Mixed | — | < 300 $\mu$m | — | — | (–) 300 4× | 5 mL (–) | Manual |
| Gyi et al. (2019) | ID, abundance, size (ESD vol) | — | — | Mixed | Formalin | — | — | Auto-image | FC100 10× | 0.14 mL min$^{-1}$, 5 FPS | (–) with VS |
| Corcoran et al. (2019) | ID, abundance, size (ABD) | Benchtop B3 series | | 2 monocultures | — | — | Diluted to ≤ 30 cells per frame | — | — | 0.2 mL (–), > 10,000 particles, 3 min | Auto (–) with VS |
| Patil and Anil (2019) | ID, abundance | — | — | Mixed | Fresh | 5–100 $\mu$m, > 100 $\mu$m | — | Auto-image | (–) 100 10×, (–) 300 4× | 2–5 mL (–) | Manual |
| Lin et al. (2019) | Size (ESD) | — | — | Mixed | Lugol's, Paraformaldehyde | — | Concentrated | Auto-image | (–)100 10×, (–) 300 4× | 2–3 × 2–5 mL processed | Manual with VS |
| Plummer et al. (2019) | Size (ABD, ESD, FD) | Color | — | Monoculture | — | — | Diluted to × 0.167 | Fluoro-trigger (400 nm) | (–) 20× | 0.5 mL processed, 0.02 mL min$^{-1}$ | Manual with VS |
| Tseng et al. (2019*a*) | Abundance, size (L) | VS series | — | Monoculture | — | — | — | — | — | 0.3 mL min$^{-1}$ | — |
| Whalen et al. (2019) | ID, abundance | — | — | Mixed | Formalin | < 200 $\mu$m | — | Auto-image | (–) 300 (–) | ~90 mL (–), 5–10,000 particles, 2 mL min$^{-1}$ | — |
| Lomas et al. (2019) | Abundance, size (SB)* | VS series benchtop | — | 11 monocultures | Bouin's | — | — | Auto-image | (–) 200 10× | — | (–) with VS |
| Feng et al. (2019*a*) | Size (L) | VS4 | — | Mixed | Fresh | 100–300 $\mu$m | Concentrated to × 20 | Auto-image | (–) 300 4× | 2–10 mL (–), 0.4 mL min$^{-1}$, 2 min, 5 FPS | — |
| Solomon et al. (2019) | ID, abundance | — | — | Mixed | Fresh | — | — | Auto-image | FOV100 10× | 10 mL (–), 0.3 mL min$^{-1}$ | Auto with VS, then manual |
| Park et al. (2019*b*) | Imaging | — | — | Mixed | — | — | — | — | (–) 4× | 1922 particles | Auto with external |
| Wang et al. (2019) | ID, abundance, size (L) | VS4 | — | Mixed | Fresh | 63–250 $\mu$m | — | Auto-image | FC300 4× | 1 mL processed, 0.4 mL min$^{-1}$, 2 min, 5 FPS | — |
| Lombard et al. (2019) | Size (ESD) | — | — | Mixed | — | > 20 $\mu$m | — | — | (–) 20× | — | Manual |
| Tseng et al. (2019*b*) | Abundance*, size (ABD vol) | VS series | — | Monoculture | — | — | — | — | — | 0.3 mL (–), 0.3 mL min$^{-1}$ | — |
| Pattullo et al. (2019) | Abundance | Benchtop | — | Monoculture | — | — | — | Auto-image | — | — | — |
| Wirth et al. (2019) | Abundance, size (L, W) | — | 3.7.5 | 2 monocultures | Fresh | — | — | Fluoro-trigger (532 nm) | FOV80 10× | 0.15 mL min$^{-1}$ | (–) with VS |
| Black et al. (2019) | ID, abundance | Benchtop B3 series | 3.4 | Mixed | Glutaraldehyde | Centrifuged to remove sediment | Diluted to × 0.02 | — | — | 1 mL imaged | — |

*(Continues)*

**Table 1.** Continued

| Reference | FlowCam used for | FlowCam model | VS version | Sample composition | Sample preservation | Sample pre-filtration | Sample concentration or dilution | FlowCam processing mode | Flow cell, objective lens | FlowCam processing details | Image sorting method |
|---|---|---|---|---|---|---|---|---|---|---|---|
| Viana et al. (2019) | Abundance, size (L, W) | — | | Mixed | Fresh | < 100 $\mu$m | — | Auto-image | FOV90 10× | 0.1 mL min$^{-1}$, 20 min, 20 FPS | Auto with VS, then manual |
| Anderson and Harvey (2019) | ID, abundance, size (L, W) | — | — | Mixed | Formalin | < 200 $\mu$m | — | Auto-image | (–) 300 (–) | ~27,000 particles, 2 mL min$^{-1}$ | — |
| Baer et al. (2019) | ID, abundance, size (–) | — | — | Mixed | Fresh | > 20 $\mu$m | Concentrated to × 80–160 | Fluoro-trigger (488 nm) | (–) 200 4× | — | — |
| Hasberg et al. (2019) | Abundance | Benchtop B3 series VS | — | Mixed | Hydrogen peroxide | < 25 $\mu$m, 25–80 $\mu$m, > 80 $\mu$m | Diluted, diluted with 2% PVP | — | (–) 100 10×, (–) 100 10×, (–) 300 4× | — | Auto (–) |
| Nolan and Cardinale (2019) | Size (ABD) | Benchtop | — | Mixed | — | — | — | — | — | ≥ 70 particles | — |
| Feng et al. (2019*b*) | ID, abundance, size (L) | VS4 | — | Mixed | — | 35–40 $\mu$m, 40–100 $\mu$m, 100–300 $\mu$m | Concentrated | Auto-image | FC50 20×, FC100 10×, FC300 4× | 0.05–0.4 mL min$^{-1}$, 2–5 min, 5–20 FPS | — |
| Woods et al. (2018) | ID, abundance | VS series, 12.5-mL syringe | — | Monoculture | — | — | — | — | FOV1000 2× | 10 mL min$^{-1}$, 18 FPS | — |
| Wang et al. (2018*b*) | Size (–) | VS4 | — | Mixed | Fresh | — | — | Auto-image | FC100 10× | 1 mL (–), 0.5 mL min$^{-1}$, 20 FPS | — |
| Bergkemper and Weisse (2018) | ID, size (ABD, L, W) | — | 3.7.5 | Mixed | Fresh | < 200 $\mu$m | | Fluoro-trigger (532 nm) | FOV80 10× | 0.15 mL min$^{-1}$ | — |
| do Rosario Gomes et al. (2018) | Abundance | — | — | 4 monocultures | Lugol's | — | — | — | — | 5 mL processed | — |
| Bernhardt et al. (2018*a*) | Abundance, size (ABD) | VS series | — | Monoculture | — | — | — | — | — | 0.3 mL min$^{-1}$ | — |
| Graham et al. (2018) | Abundance, size (ABD) | Benchtop VS-IV, autofocus | 3.8.2 | Mixed | Lugol's | None | None | Auto-image | (–) 50 20×, (–) 100 10× | 0.035–0.2 mL processed, 0.02 mL min$^{-1}$, 20 FPS | Manual with VS |
| Mistry and Ackerman (2018) | Abundance, size (ESD) | Benchtop3 VS4 series | — | Mixed | — | < 100 $\mu$m | — | Auto-image, fluoro-trigger (488 nm) | FOV80 10× | 0.2 mL min$^{-1}$ | — |
| Roque et al. (2018) | Abundance, size (L) | — | — | Mixed | — | — | — | Auto-image | (–) 20× | 50 mL processed, 2 min | — |
| Chaffin et al. (2018*a*) | ID, size (SB, "diameter" [–]) | — | 4.0.27 | Mixed | — | — | — | Auto-image | (–) 20×, (–) 10×, (–) 4× | 8000 particles | Auto with VS, then manual |
| Greer et al. (2018) | ID, abundance, size (–) | Benchtop B3 series | | Mixed | — | — | — | — | — | — | — |
| Bernhardt et al. (2018*b*) | Abundance | VS series | — | Monoculture | — | — | — | — | — | 0.25 mL (–), 0.3 mL min$^{-1}$ | — |
| Briggs et al. (2018) | ID, abundance | — | — | Mixed | — | — | — | Fluoro-trigger (–) | (–) 300 4× | 50–100 mL (–), 2.5 mL min$^{-1}$ | Manual with VS |
| Nissimov et al. (2018) | Color ratios | — | 4.0.27 | Monoculture | Alcian blue, acetic acid | — | — | Auto-image | (–) 10× | 0.1 mL imaged, 0.1–0.08 mL min$^{-1}$, 20–30 FPS | Manual |

*(Continues)*

**Table 1.** Continued

| Reference | FlowCam used for | FlowCam model | VS version | Sample composition | Sample preservation | Sample pre-filtration | Sample concentration or dilution | FlowCam processing mode | Flow cell, objective lens | FlowCam processing details | Image sorting method |
|---|---|---|---|---|---|---|---|---|---|---|---|
| Anderson et al. (2018) | ID, abundance, size (L, W) | – | — | Mixed | Formalin | < 200 $\mu$m | — | Auto-image | (–) 300 (–) | 5–10 mL (–), 2–7000 particles, 2 mL min$^{-1}$ | — |
| Jyothibabu et al. (2018*a*) | Abundance, fluorescence | — | — | Mixed | — | — | — | — | — | 1000 mL (–) | — |
| Lampe et al. (2018) | ID, abundance | VS4 color, C71 syringe | 3.1 | Mixed | Fresh | < 300 $\mu$m | — | Fluoro-trigger (532 nm) | (–) 100 20×, (–) 300 10× | ≥ 5 mL processed, 0.2–0.3 mL min$^{-1}$ | — |
| Jyothibabu et al. (2018*b*) | Abundance, size (ABD) | — | — | Mixed | Fresh | 20–300 $\mu$m | Concentrated to × 10–50 | — | FOV300 4× | 20 mL processed, 20 min | — |
| Magonono et al. (2018) | ID** | Benchtop VS IV | — | Mixed | — | — | — | Fluoro-trigger (–) | — | — | Manual |
| Göritz et al. (2018) | ID, abundance, size (–) | VS | — | Mixed | Fresh | — | — | Auto-image | (–) 100 10×, (–) 300 4× | — | — |
| Selz et al. (2018) | ID, abundance, size (ABD, CP) | VS IVc | — | Mixed | — | < 300 $\mu$m | — | Trigger (–) | (–) 4× | 1–5 mL processed | Manual |
| Segovia et al. (2018) | ID, abundance, size (ESD, ABD) | II B/W | 1.5.16 | Mixed | Fresh, Lugol's | — | — | Auto-image | FC100 10× | 0.12 mL imaged, 9 FPS | Manual |
| Poulin et al. (2018*a*) | Abundance | — | — | Monoculture | — | — | — | — | — | — | — |
| Noh et al. (2018) | Abundance | — | — | Monoculture | Fresh | — | — | — | — | — | — |
| Kydd et al. (2018) | ID, abundance, size (ABD, ESD) | — | — | Mixed | Ethanol | 30–75, 75–295, and 295–1000 $\mu$m | None, 2.5% PVP, 2.5% PVP | Auto-image, scatter-trigger | FOV80 10×, FOV300 4×, FOV1000 2× | 3 mL processed, 20–60 min | Manual with VS |
| Chaffin et al. (2018*b*) | ID, size (SB, "diameter" [–]) | — | 4.0.27 | Mixed | — | 3–10 $\mu$m, > 10 $\mu$m | — | — | (–) 20×, (–) 10× | 8000 particles, 0.02–0.15 mL min$^{-1}$ | Auto with VS, then manual |
| Poulin et al. (2018*b*) | Abundance | — | — | Monoculture | Lugol's | — | — | Auto-image | (–) 100 (–) | 0.4 mL min$^{-1}$, 16 FPS | — |
| Kurobe et al. (2018) | Abundance, size (ABD)* | — | — | Monoculture | Lugol's | — | — | — | — | — | — |
| Wang et al. (2018*a*) | Abundance | VS4 | — | 2 monocultures | Fresh | 35–40, 40–100, and 100–300 $\mu$m | Concentrated | Auto-image | FC50 20×, FC100 10×, FC300 4× | 0.05–0.4 mL min$^{-1}$, 2–5 min, 5–20 FPS | — |
| Romero-Martínez et al. (2017) | ID, abundance*,‖, size†† (ABD, ESD, GL, GT, L, W) | Benchtop B3 series | 3.2 | Monoculture, mixed | Fresh | > 4 $\mu$m | — | Auto-image | (–) 100 10× | 0.3 mL imaged, 0.14 mL min$^{-1}$, 20 FPS | Manual with external |
| Coello-Camba et al. (2017) | Abundance | — | — | — | — | — | — | — | (–) 300 4× | — | — |
| Kayfetz and Kimmerer (2017) | Abundance*, size (L, W) | — | — | Mixed | Fresh, glutaraldehyde | — | — | Auto-image, fluoro-trigger (–) | — | 0.94 mL imaged, 20 FPS | Manual with VS |
| Hinners et al. (2017) | Size (–) | VS IV | — | Monoculture | Lugol's | — | — | — | — | 7 mL processed | — |

*(Continues)*

**Table 1.** Continued

| Reference | FlowCam used for | FlowCam model | VS version | Sample composition | Sample preservation | Sample pre-filtration | Sample concentration or dilution | FlowCam processing mode | Flow cell, objective lens | FlowCam processing details | Image sorting method |
|---|---|---|---|---|---|---|---|---|---|---|---|
| Arrigo et al. (2017) | ID | — | — | — | — | — | — | — | — | — | — |
| Fileman et al. (2017) | Abundance, size (–) | VS IV-C, syringe | 3.2.3 | Mixed | Lugol's | 10–100 $\mu$m | Concentrated to $\times$ 2.5 | Scatter-trigger | (–) 100 10× | — | (–) with VS |
| de-los-Ríos-Mérida et al. (2017) | Abundance, size (ESD) | — | — | Mixed | Formalin | — | None | Auto-image | (–) 100 10× | — | Manual |
| Karnan et al. (2017*a*) | ID, abundance, size (ABD) | Portable | 2.4 | Mixed | Formalin | 0.2–1 mm, > 1 mm | Concentrated | Auto-image | FOV1000 2×, FOV2000 2× | — | Manual with VS |
| Karnan et al. (2017*b*) | ID, abundance, size (ABD†) | — | 2.4 | Mixed | — | 20–300 $\mu$m | Concentrated to $\times$ 10 | Fluoro-trigger (–) | FOV300 4× | — | Manual with VS |
| Stamieszkin et al. (2017) | ID, abundance, size (ABD) | VS IV | — | Mixed | Fresh | — | — | Fluoro-trigger (532 nm) | (–) 3000 4× | 150 mL (–) | Auto with VS, then manual |
| Keys et al. (2017) | ID | — | — | Mixed | Lugol's | 18–100 $\mu$m | Concentrated | — | — | 250 mL (–) | |
| Yang et al. (2017*a*) | Size (ESD*,††) | VS-IV, 1024 × 768 | 2.4.8 | 3 monocultures | Lugol's, formalin | — | — | Auto-image | (–) 4× | 60–300 particles | Manual |
| Milde et al. (2017) | Abundance, size (ABD area, E, ESD, ESD vol, R, S, W) | — | — | Mixed | Ethanol | 53–300 $\mu$m | — | Auto-image | — | 8–15,000 particles, 1.75 mL min$^{-1}$, 20 FPS | — |
| Bishop and Spaulding (2017) | Size (–) | Benchtop VS-IV | — | Monoculture | Hydrogen peroxide | — | — | — | (–) 10× | 300–2400 particles | Auto with VS, then manual |
| Bergkemper and Weisse (2017) | ID, abundance | — | 3.7.5 | Mixed | Fresh | < 200 $\mu$m | — | Fluoro-trigger (532 nm) | FOV80 10× | 0.15 mL min$^{-1}$ | (–) with VS |
| Pree et al. (2017) | ID, abundance | II, black and white | — | Mixed | Fresh | — | — | Auto-image | (–) 10× | 30 min | Manual |
| Smith et al. (2017) | ID | — | — | Mixed | — | — | Concentrated to $\times$ 5 | — | — | 1 mL imaged | — |
| Patil et al. (2017) | Size (ESD, L, W) | — | — | Mixed | Fresh | 5–100 $\mu$m | — | Auto-image | (–) 100 10× | 2–5 mL (–) | Manual |
| Franzè and Lavrentyev (2017) | Size* (–) | — | — | Mixed | Formaldehyde | — | Concentrated to 1 particle per frame | Fluoro-trigger (650 nm) | — | Flow rate to 1 particle per frame | — |
| Natunen et al. (2017) | Abundance, lipid detection | Benchtop B2, peristaltic pump | 2.4.1 | Monoculture | Fresh, Nile red stain | — | None, diluted to ~35,000 cells mL$^{-1}$ | Auto-image, fluoro-trigger (532, 575 nm) | (–) 100 10×, (–) 100 20× | 20–400 particles, 0.3 mL min$^{-1}$, 2 min | Manual |
| Giling et al. (2017) | ID* | — | — | Mixed | Fresh | — | — | — | — | — | — |
| Hassett et al. (2017) | ID, abundance | Benchtop VS | — | Mixed | Ethanol | 64–280 $\mu$m | Diluted to × 0.05, added 2 mL glycerin | Auto-image | (–) 300 4× | 1 mL processed | Auto with VS, then manual |
| Lehman et al. (2017) | ID, size (ABD) | — | — | Mixed | Lugol's, fresh | 75–300 $\mu$m, > 300 $\mu$m, > 10 $\mu$m | — | —, Fluoro-trigger (–) | (–) 10×, (–) 4×, (–) 100 10× | 10 min | — |
| Yang et al. (2017*b*) | ID, abundance*, size (ABD, L*, W) | — | — | Mixed | Formaldehyde | 76–600 $\mu$m | — | Auto-image | — | — | Auto (–), then manual |

*(Continues)*

**Table 1.** Continued

| Reference | FlowCam used for | FlowCam model | VS version | Sample composition | Sample preservation | Sample pre-filtration | Sample concentration or dilution | FlowCam processing mode | Flow cell, objective lens | FlowCam processing details | Image sorting method |
|---|---|---|---|---|---|---|---|---|---|---|---|
| Muñoz et al. (2017) | Size (ESD, "size," "area," "shape" [–]) | — | — | Mixed | Formaldehyde | 53–300 $\mu$m | Concentrated | Auto-image | FOV300 4× | — | Manual |
| Segovia et al. (2017) | ID, abundance, size (–) | — | — | Mixed | Fresh | — | — | Auto-image | (–) 300 4× | 6.3 mL (–), flow rate to 1 particle per frame | — |
| Goulet et al. (2017) | ID, abundance | — | — | Monoculture | — | — | — | — | — | 3 × 0.1 mL (–) | Manual with VS |
| Álvarez et al. (2017) | Abundance*, size (ESD), fluorescence | Onboard | — | Mixed | Fresh | < 40 $\mu$m, < 100 $\mu$m | Concentrated to × 50 | Fluoro-trigger (488, 650 nm) | FC50 20×, FC100 10× | 10 mL (–), 30 min | Auto with external |
| Omar et al. (2017) | ID, abundance | Benchtop VS | — | Mixed | — | — | — | — | — | — | — |
| Wang et al. (2017) | ID, abundance†† | Benchtop B3 series | 3.4 | Monoculture | — | — | — | Auto-image | FC300 4× | 1.0 mL min$^{-1}$ | — |

ABD, area-based diameter, one of the FlowCam particle measurement outputs ($\mu$m); ABD area, one of the FlowCam particle measurement outputs calculated based on ABD ($\mu$m$^2$); ABD vol, ABD volume, one of the FlowCam particle measurement outputs calculated based on ABD ($\mu$m$^3$); AR, aspect ratio, one of the FlowCam particle measurement outputs; CP, convex perimeter, one of the FlowCam particle measurement outputs ($\mu$m); E, elongation, one of the FlowCam particle measurement outputs; ESD, equivalent spherical diameter, one of the FlowCam particle measurement outputs ($\mu$m); ESD vol, ESD volume, one of the FlowCam particle measurement outputs calculated based on ESD ($\mu$m$^3$); FC/FOV, standard flow cell (FV) or field-of-view flow cell (FOV); FD, filled diameter, one of the FlowCam particle measurement outputs ($\mu$m); FPS, frames per second, a measure of frame rate for FlowCam image acquisition; GL, geodesic length, one of the FlowCam particle measurement outputs ($\mu$m); GT, geodesic thickness, one of the FlowCam particle measurement outputs ($\mu$m); L, feret length, one of the FlowCam particle measurement outputs ($\mu$m); PVP, polyvinylpyrrolidone, a product which Yokogawa Fluid Imaging Technologies sells as an optional gelling agent to slow particle movement through the FlowCam; R, roughness, one of the FlowCam particle measurement outputs; S, symmetry, one of the FlowCam particle measurement outputs; SB, shape-based biovolume: biovolume (cylinder), biovolume (sphere), or biovolume (p. spheroid); a series of FlowCam particle measurement outputs selected based on particle morphology ($\mu$m$^3$); VS, *VisualSpreadsheet*, the FlowCam software used to control the device and to manually, automatically or semi-automatically sort collected images; W, feret width, one of the FlowCam particle measurement outputs ($\mu$m).

*Calibrated against or compared to light microscopy.

†A reason was provided for the selection of the size measurements.

‡Calibrated against or compared to Imaging FlowCytobot.

§Calibrated against or compared to 4Deep HoloSea holographic microscope.

‖Calibrated against or compared to flow cytometry.

¶Calibrated against or compared to Coulter Counter.

#Calibrated against or compared to LISST-100X or LISST-200X (Laser In-Situ Scattering and Transmissometery).

**Taxonomic identification confirmed by molecular techniques.

††Cell density or size measurements confirmed by comparing to calibration beads.

**Table 2.** Summary of methods reported in papers using FlowCam to image phytoplankton published between 2017 and 2020 ($n = 116$).

| Methods detail included | Proportion of papers (%) |
|---|---|
| Any FlowCam model details | 47 |
| Any sample preparation methods | 78 |
| FlowCam processing mode | 67 |
| FlowCam flow cell and objective | 53 |
| Any FlowCam settings used to process samples | 49 |
| Post-processing technique (manual and/or automated image sorting) | 47 |
| Post-processing software used | 35 |
| Specific measurement outputs used (for those using measurement outputs)* | 79 |
| Justification for measurement output choice (for those using measurement outputs)* | 40 |

*Proportions here calculated from the 65% of studies which reported using measurement outputs ($n = 75$).

images have many more distinguishable shades than grayscale images, and color FlowCam units output six additional color-based particle properties). One study did, however, state the year of manufacture and serial number of their unit (Kimambo et al. 2020). This detail allows readers to pinpoint those studies that have been performed using the same FlowCam unit.

### Sample composition and preparation

The quality, reliability, and reproducibility of FlowCam outputs are also directly affected by the sample composition and the preparation and preservation methods used prior to processing those samples through the FlowCam. While insufficient details on the context and preparation of samples is also a widespread issue throughout traditional approaches like manual microscopy (Marqués et al. 2020; Heddleston et al. 2021), there are several key details that affect FlowCam outputs specifically. Several studies have found that sample composition (taxonomy, cell size, cell density, or sediment presence) can impact the accuracy of FlowCam automated cell density estimates (Littman et al. 2008; Bergkemper and Weisse 2017; Graham et al. 2018; Hrycik et al. 2019; Menden-Deuer et al. 2020). As FlowCam samples are passed through a thin tube (the *flow cell*) ranging from 50 to 2000 $\mu$m depth, samples generally require some form of pre-filtering to avoid clogging-related issues (Poulton and Martin 2010; Poulton 2016). Most of the 116 reviewed studies did not report any pre-filtering of samples prior to processing (62%). It is unclear whether any pre-filtering occurred for these samples and, if not, if the presence of any particles or clusters of particles wider than the flow cell led to clogging of the flow cell, which is known to impact findings (Graham et al. 2018). For mixed phytoplankton samples, better processing performance and quality images can also be acquired by serially filtering samples, so that different phytoplankton size classes can be imaged separately using a series of differently sized flow cells and microscope objectives (Poulton and Martin 2010; Patil and Anil 2015; Poulton 2016), but this was reported by only three of the 116 studies. The inclusion of

**Table 3.** FlowCam technical specification options. This information was obtained directly from Yokogawa Fluid Imaging Technologies marketing information, via communication with Yokogawa Fluid Imaging Technologies staff and with staff from their Australian distributor, Kenelec Scientific.

| Technical specification | Options |
|---|---|
| Model number | B1, B2, B3, VS-I, VS-II, VS-III, VS-IV (for B- and VS-series, benchtop, or onboard), 8100, 8400, Cyano, Nano, Macro, 5000 |
| Production year | 1998 to present |
| Image acquisition mode | Auto-image mode, scatter-triggered mode, and/or fluorescence-triggered mode (488, 532, and/or 633 nm lasers) |
| Focus | Manual focus or autofocus |
| Fluidics | Peristaltic pump, syringe pump (0.5, 1.0, 5.0, or 12.5 mL) or Automated Liquid Handling (ALH) system |
| Camera resolution | 1024 × 768, 1280 × 960 or 1920 × 1200 pixels |
| Camera color | Monochrome or color |
| Maximum frame rate | 11, 22, 60, or 120 FPS |
| Objective options | 2×, 4×, 10×, and/or 20× |
| Flow cell options | Standard: 50, 100, 200, 300, 600, 800, 1000, 2000 $\mu$m |
| | VS-series FOV: 80, 300, 1000 $\mu$m |
| | 8000-series FOV: 50, 80, 100, 300, 600, 1000 $\mu$m |

method steps such as serial filtering of samples substantially influences the human resourcing time to process samples with FlowCam, an important factor for routine monitoring programs potentially wishing to compare resourcing requirements of such technologies against more traditional sample processing methods.

Depending on sample composition and the FlowCam image capture mode used, sample concentration may need to be adjusted as auto-image mode works best with dense samples (limited only by overlapping particles), while fluorescence-triggered mode requires dilute samples (maximum of one particle per frame) (Sieracki et al. 1998; Poulton and Martin 2010; Poulton 2016). Graham et al. (2018) found that FlowCam auto-imaged cell density estimates of cyanobacteria were significantly similar to microscopy estimates only when the cell density was $< 100{,}000$ cells $mL^{-1}$. When working with monocultures, Romero-Martínez et al. (2017) found that cell concentrations in samples run through the FlowCam needed to be sufficiently high to minimize the bias caused by non-target particles including bubbles. Concentration techniques can affect sample composition (Hötzel and Croome 1999), and dilution techniques should clearly specify the substance used for dilutions and its possible impact on FlowCam outputs (addition of further non-target particles). However, only 34% of studies stated whether samples were concentrated, diluted, or kept at their initial concentration.

Preservation of phytoplankton samples can affect the size and features (including shape) of cells and can lead to inequal cell losses (Menden-Deuer et al. 2001; Rutten et al. 2005; Zarauz and Irigoien 2008). Moreover, it can also affect the capture settings that can be used on the FlowCam, as most preservation methods will prohibit the use of the fluorescence-triggered capture mode (Poulton and Martin 2010; Poulton 2016). Preservation with Lugol's iodine solution has also been found to significantly increase FlowCam cell counts by reducing adhesion of cells to the flow cell and increasing identification rates when compared to fresh samples (Graham et al. 2018). Despite this, approximately a third (34%) of the reviewed studies failed to state whether samples were preserved, even for those that used FlowCam to measure cell size (31%).

**FlowCam setup and processing settings**

The quality of images captured by the FlowCam will directly impact the accuracy of any outputs derived from it (Camoying and Yñiguez 2016; Bergkemper and Weisse 2017). While with manual microscopy the operator can adjust focus and even rotate individual cells to view key identifying features, each cell in a FlowCam analysis is at best characterized by one automatically captured, two-dimensional digital image. If the FlowCam is used to assess the taxonomic or size-based composition of a sample, then it needs to be confirmed to be capturing an accurate representation of that sample. The mechanics of FlowCam analysis, with samples pulled through a narrow flow cell, mean that some individuals may be more prone to exclusion, clogging, or adhesion to the flow cell surface (Graham et al. 2018; Mistry and Ackerman 2018). Capturing images of cells from only one direction results in the key identifying features of some taxa being missed. Given that the microscope lens and digital camera can only be perfectly focused on one plane within the flow cell (which has a depth from 50 to 2000 $\mu$m), a proportion of images will always be out of focus to some degree (Romero-Martínez et al. 2017). The flow rate and cell density need to be perfectly balanced for every sample to avoid either additional blurry images due to excessively high flow speeds, or duplicate images of the same cells if flow speeds are too low (Natunen et al. 2017; Nissimov et al. 2018). Similarly, shutter speed, gain, and intensity need to be carefully balanced to reduce blurriness of images while also maintaining appropriate brightness and contrast to maximize image quality and the observability of key identifying features (Bayer et al. 2001; Heddleston et al. 2021).

Most FlowCam models can be equipped with up to four objective lenses (2×, 4×, 10×, and 20×), each of which can be paired with a range of different flow cell sizes and types, with the specific combination of objective and flow cell directly affecting image quality (Camoying and Yñiguez 2016). Graham et al. (2018) found that both manually identified species richness estimates and FlowCam cell density estimates varied significantly between different FlowCam objectives (4×, 10×, and 20×), with the 20× objective able to detect smaller genera that were missed at the lower magnifications. Three different flow cell types have been introduced to date: the standard flow cells (eight sizes from 50 to 2000 $\mu$m for the B- or VS-Series FlowCams), 1$^{st}$-generation field-of-view (FOV) flow cells (three sizes from 80 to 1000 $\mu$m for the VS-Series), and 2$^{nd}$-generation FOV flow cells (six sizes from 50 to 1000 $\mu$m for the 8000-Series). The FOV flow cells allow the digital camera to image the entire width of the flow cell, leading to a better capture of particles in the sample and therefore a more accurate representation of cell density. As the FlowCam B- or VS-Series models can be equipped with either a standard or FOV flow cell, it is vital that studies clearly state which style of flow cell was used. Yet, 47% of the reviewed studies did not report which flow cells and objectives they used, and 78% of studies published after the release of FOV flow cells in 2016 did not state whether they used standard or FOV flow cells.

Although it is standard practice for microscopic analyses to count or measure phytoplankton until a minimum specified number of individuals have been considered (Hötzel and Croome 1999), there are various ways to measure the amount of sample analyzed by the FlowCam to ensure representativeness and reproducibility. While only 58% of studies reported any measure of sample size, the measure reported by these studies varied, with some reporting the volume of sample run through the FlowCam (36%), the subset of that volume imaged by the FlowCam (14%), the sample processing time

(22%) or the number of particles imaged (30%). Several factors would affect the true sample size for the above measures, including cell concentration, sample flow rate, and frame rate, yet the reporting of these details is inconsistent and infrequent (Table 1). Around half (52%) of the studies presenting sample size as a volume failed to specify if this was the volume *processed* through the FlowCam or the subset of this which was *imaged* by the FlowCam, which can be anywhere from 30% to 95%, depending on FlowCam unit, flow cell, objective, flow rate, and frame rate (Poulton and Martin 2010; Álvarez et al. 2011; Camoying and Yñiguez 2016). This can be important from a metadata standpoint as inclusion criteria to plankton image dataset repositories specifically require reporting of the volume imaged (Neeley et al. 2021).

Several FlowCam studies have reported that, even when manually classified, the images produced by the FlowCam do not provide comparable plankton sample composition outputs to those obtained from traditional microscopic analyses (Brzezinski et al. 2011; Le Bourg et al. 2015). In contrast, other studies have found FlowCam outputs to be comparable to microscopy, although generally with lower taxonomic resolution (Vaillancourt et al. 2004; See et al. 2005; Ide et al. 2008), or in some cases with higher taxonomic resolution (Kydd et al. 2018; Hrycik et al. 2019). It is difficult to tease out what may have caused these conflicting results, due to the typically limited descriptions of methods across studies. As such, any studies relying solely on the FlowCam to quantify sample composition should ideally have validated their FlowCam results (considering their unique samples, FlowCam unit and methods) against the existing trusted benchmark of manual microscopy. Most studies reporting FlowCam sample composition outputs do so without any form of independent validation against microscopy or any other technique (89%).

The same issue applies to FlowCam automated cell density outputs, as these are automatically derived from the volume pumped through the flow cell and the proportion of this volume theoretically within the field of view and imaged. Some studies have found these automated cell density values are sufficiently similar to microscopy, within 20% variation (Álvarez et al. 2011; Lehman et al. 2017; Tseng et al. 2019*b*), while others have found them to over- or underestimate density, with FlowCam estimates up to 2.6 times lower or 5.5 times higher than microscopic counts of the same samples (Littman et al. 2008; Bergkemper and Weisse 2017; Kydd et al. 2018). Yu (2019) presents a Matlab-based toolkit, *FlowDensi*, which converts FlowCam outputs into more accurate density estimates. Despite this, 81% of studies reporting FlowCam-derived cell density values did so without specifying if these were taken directly from FlowCam outputs or calculated separately, following correction for any bias. Additionally, the specific operating mode applied while using the FlowCam (reported by only 67% of studies) has been shown to affect the accuracy of size structure estimates, with auto-image and fluorescence-triggered mode found to be more accurate than side-scatter triggered (Álvarez et al. 2011). The length of tubing left attached to the flow cell (reported by 0% of studies) can also impact cell density estimates, with shorter tubing reducing cell adhesion and blockages (Edwards et al. 2017). The accuracy of FlowCam cell density and size structure estimates is affected by sample composition (Álvarez et al. 2011; Menden-Deuer et al. 2020); but also by FlowCam set up details (flow cell size and type, objective magnification, tubing length) and processing settings (operating mode, flow rate, frame rate), and so should be validated in every unique case.

**FlowCam image post-processing**

The initial FlowCam output is comprised of thousands of automatically cropped images of individual particles, each with a set of automatically generated measurements. Image outputs can include a range of non-target particles such as detritus, bubbles, cellular debris, duplicate cells, and image artifacts such as overlapping particles, unidentifiable blurry particles and particles partially out of frame (Nissimov et al. 2018; Patil and Anil 2019; Menden-Deuer et al. 2020). Depending on sample type, non-target images can represent up to 95% of image outputs (unpublished data), and even when imaging just purified (Milli-Q) water as a blank FlowCam outputs have recorded 98 non-target images (dust and bubbles) per mL processed (Romero-Martínez et al. 2017). The FlowCam is unable to differentiate target from non-target particles without post-processing of images, as even in fluorescence-triggered mode any particle in the frame when fluorescence is detected will be imaged and individually cropped (Álvarez et al. 2012). With traditional manual microscopy the taxonomist would not consider any non-target particles, thus these images need to be removed from FlowCam datasets with some form of image post-processing. Yet, almost half of studies do not describe any post-processing of images (45%), leaving readers unclear on the potential impacts of non-target images on the study outputs and conclusions.

Although the FlowCam is reportedly able to automatically sort collected images through its associated *VisualSpreadsheet* and *Classifier Advanced* software packages, most studies do not make use of these capabilities (89%), using the FlowCam only as a means to collect digital images and/or measurements of phytoplankton which are either not explicitly sorted (45%), sorted manually (32%), auto-sorted using external software (4%), or the method of sorting is unclear (9%). Where a sorting method is either not stated or not clearly stated (53%) a reader may mistakenly presume samples have been successfully auto-classified using the advertised FlowCam capabilities, but even those explicitly using *VisualSpreadsheet* for auto-classification (11%) relied on it only as a first-pass pre-sorting before manual correction.

Auto-classifications by both *VisualSpreadsheet* and *Classifier Advanced* use supervised image sorting techniques, requiring

the user to first create extensive *image libraries* of manually classified images, which are then used by the software for auto-classifications using a series of user-defined *filters* (a set of specific software settings and *particle properties* that are extracted from and used to classify each new image). The descriptions of *VisualSpreadsheet* auto-classification methods varied considerably between the 13 studies using it for first-pass sorting; eight provided no details, four stated the number of libraries, two stated the number of images per library and one stated the particle properties used in filters. Just one of these studies provided an estimate of accuracy, stating that classifications were only correct in half of the cases (Hassett et al. 2017), but this was one of six studies that failed to specify which version of *VisualSpreadsheet* was used.

Extending the literature search outside of 2017–2020, only three studies have considered *VisualSpreadsheet* as a method to auto-classify phytoplankton samples as a one-step method (Buskey and Hyatt 2006; Camoying and Yñiguez 2016; Mirasbekov et al. 2021). Buskey and Hyatt (2006) concluded that a two-step auto-then-manual method was still required, while Camoying and Yñiguez (2016) and Mirasbekov et al. (2021) concluded that *VisualSpreadsheet* auto-classifications had relatively high accuracy compared to microscopy, even down to genus or species level. All three studies provided assessments of their auto-classification accuracies but were missing some key method details required to allow for full interpretation of these results. Each paper omitted the FlowCam model or technical specifications and version of FlowCam software used for analyses, Buskey and Hyatt (2006) did not explain which settings or particle properties were selected for filters, and Camoying and Yñiguez (2016) did not list how many images were in each image library.

To further highlight the potential effects of these methods considerations on FlowCam auto-classifications, the following case study was conducted to quantify the impacts of (i) FlowCam software choice, (ii) image library size, and (iii) filter particle property selections on auto-classification accuracy.

***Case study 1***

The FlowCam used for the following analyses was a FlowCam VS-I, updated in 2013 to posess a $1280 \times 960$ pixel color camera and 0.5-mL syringe pump. Lugol's-stained cultures of two morphologically distinct phytoplankton (the ovoid *Amphidinium carterae* [hereafter referred to as Species A], and the elongated *Ankistrodesmus* sp. [Species B]) were processed in auto-image mode through a 50 $\mu$m standard flow cell (FV50) and 20$\times$ objective (full methods details and example images provided in Supporting Information Appendix B). Images collected by running these monocultures were used to create image libraries for both species containing 50, 500, and 5000 clear images each. Four test sets were then created by imaging four mixed samples of the two species and manually selecting 250 clear images of each species, so that each test set contained exactly 500 clear images with a 1 : 1 ratio of Species A and Species B. Additional test sets were also created with 500 clear images of only Species A and only Species B (1 : 0 and 0 : 1 ratio), with the findings for these test sets presented in Supporting Information Appendix B.

To determine the impact of software type and library size, both FlowCam software packages, *VisualSpreadsheet* (Version 4.12.3) and *Classifier Advanced* (Version 1), were tested with all three library sizes using default filter settings and all 27 relevant particle properties selected. In addition, to determine the impact of filter particle property selections, 4 different combinations of particle property settings were tested; the 27 most relevant, the 11 used by Camoying and Yñiguez (2016), the 3 most relevant and the 1 most relevant (see Supporting Information Appendix B for further explanation of particle property selections), using *VisualSpreadsheet* and only the 500-image libraries. In all cases the performance of the auto-classifications was assessed by manually checking the FlowCam outputs and recording the number of images correctly assigned to Species A or B, incorrectly assigned to Species A or B, and incorrectly rejected as being neither Species A nor B (the software will "reject" images that it deems should not be assigned to any of the provided image libraries).

The results indicate that the number of images included in FlowCam image libraries directly impacts the accuracy of auto-classifications performed using both *VisualSpreadsheet* and *Classifier Advanced* software packages, with larger libraries generating more accurate classifications (Fig. 1a,b). They also highlight that auto-classification results differ between *VisualSpreadsheet* and *Classifier Advanced*, even where the exact same image libraries, test sets, and settings are used, with *Classifier Advanced* generally performing more accurately (cf. Fig. 1a,b). Within *VisualSpreadsheet*, the filter settings selected (i.e., the number and type of particle properties used by the algorithm for auto-classification) also directly impact auto-classification accuracy, with greater accuracy observed for lower numbers of particle properties (Fig. 1c). Together, these results highlight the importance of detailed methods descriptions and validations for studies making use of the FlowCam auto-classification capabilities.

**Use of FlowCam outputs**

In addition to capturing images of particles as they flow through the FlowCam, the instrument's *VisualSpreadsheet* software automatically collects up to 47 particle properties for every image, including several that may be informative for understanding phytoplankton ecology (measures of cell size, shape, and volume). The distribution of individual cell sizes can be an important indicator of phytoplankton community structure and function, and the total biovolume or biomass of phytoplankton can provide a valuable alternative representation to simpler count-based measures (McCauley and Kalff 1981; Falkowski and Oliver 2007; Marañón et al. 2012, 2013). Cell biovolume can also be converted to represent

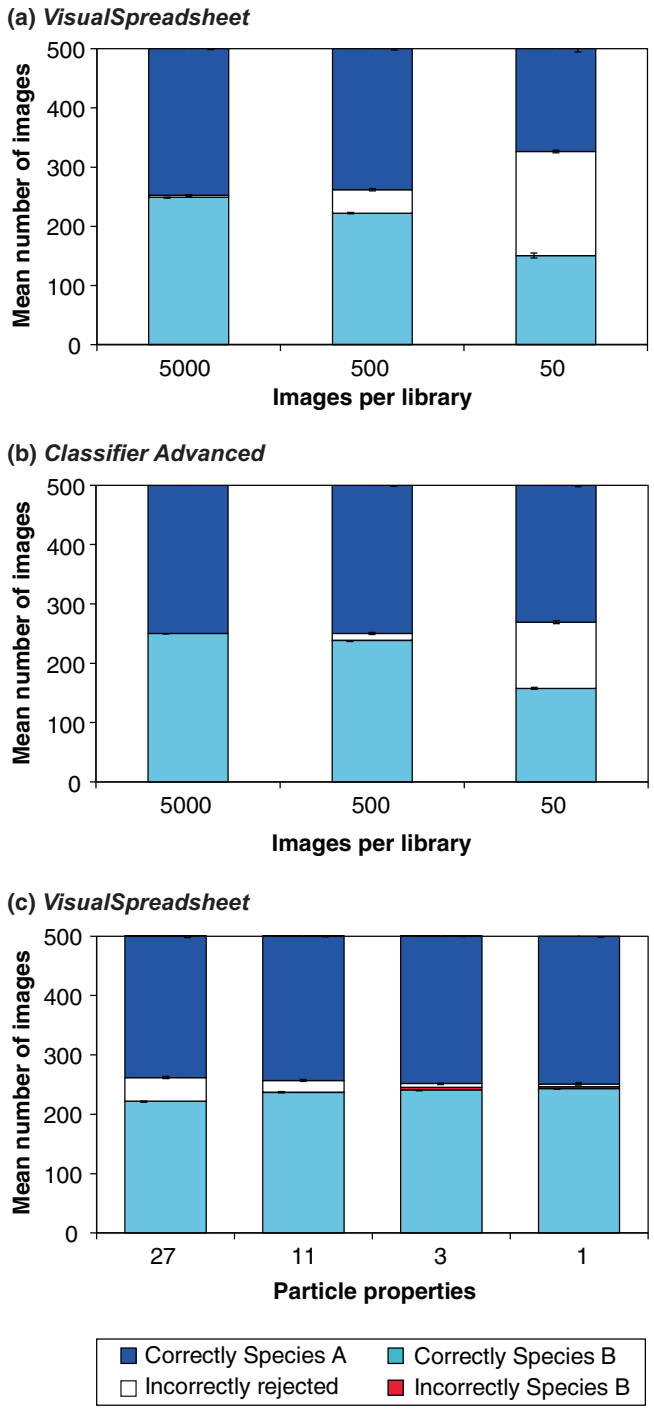


**Fig. 1.** Mean manually checked FlowCam auto-classification results for test sets with exactly 250 clear images of Species A (*Amphidinium carterae*) and 250 clear images of Species B (*Ankistrodesmus* sp.), comparing (**a**) the number of images used in libraries for auto-classifications (using *VisualSpreadsheet* software and 27 particle properties), (**b**) the number of images used in libraries for auto-classifications (using *Classifier Advanced* software and 27 particle properties), and (**c**) the number of particle properties selected in filters for auto-classifications (using *VisualSpreadsheet* software and 500-image libraries). Error bars represent the Standard Error, $n = 4$ test sets. Note no images were incorrectly assigned as Species A.

**Table 4.** FlowCam measurement outputs reported as used by papers using FlowCam to image phytoplankton between 2017 and 2020 ($n = 75$).

| Measurement outputs | Proportion of papers (%) |
|---|---|
| ABD diameter | 36 |
| ESD diameter | 27 |
| Length | 24 |
| Width | 17 |
| Shape-based biovolume (biovolume [cylinder, sphere, and p. spheroid]) | 11 |
| Geodesic length and thickness | 3 |
| ESD volume | 3 |
| ABD volume, aspect ratio, convex perimeter, elongation, FD diameter, roughness, symmetry (used once each) | 1 |
| Unclear | 7 |
| No measurement outputs reported | 29 |

carbon or other elemental content and is valuable in understanding the role of phytoplankton in biogeochemical cycles and increasingly in the field of blue carbon sequestration (Dunne et al. 2007; Lovelock and Duarte 2019). As the FlowCam can calculate these measures in a far more time-efficient manner than traditional manual microscopy, most reviewed studies (65%) have used the FlowCam to collect data on phytoplankton size.

Eighteen different output metrics were used across these studies (Table 4), with the most popular being *ABD diameter* (hereafter ABD), *ESD diameter* (hereafter ESD), *length*, *width*, and shape-based biovolume measures (*biovolume* [*sphere*], *biovolume* [*cylinder*], and *biovolume* [*prolate spheroid*]). Several studies have compared FlowCam measurement outputs to microscopy or to other measurement devices such as the Coulter Counter or LISST instruments. Some studies have found these outputs to be generally comparable (Sieracki et al. 1998; Vaillancourt et al. 2004; Spaulding et al. 2012), while others have found the outputs to differ significantly between analytical approaches (Reynolds et al. 2010; Brzezinski et al. 2011; Jakobsen and Carstensen 2011; Romero-Martínez et al. 2017), or others yet have found some FlowCam outputs to be similar while others differ significantly (Hrycik et al. 2019; Wu et al. 2020*b*).

FlowCam outputs should only be used quite deliberately with a full understanding of how they are derived. Traditional microscope-based measures of cells will usually rely on just a single length and width measure (Hillebrand et al. 1999; Olenina 2006). The two most popular *VisualSpreadsheet* measures are computed quite differently; ABD is the diameter of a

circle with the same area as the *ABD area* (which is determined by the number of dark pixels in the particle, excluding inner light pixels), while ESD is the mean value of 36 equally spaced feret measurements of the particle (feret measurements are the perpendicular distance between two parallel lines touching either side of the particle). This means that ABD would be expected to underestimate the size of particles with internal transparent components, while ESD would be expected to overestimate the size of particles with protrusions or flagella. Most studies (73%) that used either *VisualSpreadsheet* ESD or ABD did not present any justification for their choice, even when comparing or combining their results with those measured using traditional microscopy (e.g., Lombard et al. 2019; Zhang et al. 2019). Four studies (5%) stated they used a "diameter" output, without stating which of the three different *VisualSpreadsheet* diameter options this was: ABD, ESD, or *FD diameter* (which is calculated much like ABD, except all light and dark pixels in the cell are included). A third (36%) of studies using FlowCam to represent cell size did not clearly state which measurement outputs they used.

Newer versions of *VisualSpreadsheet* (Version 4.0.0 and above) provide additional automated measurement outputs including a set of shape-based "biovolume" measures, *biovolume* (*cylinder*), *biovolume* (*sphere*), and *biovolume* (*p. spheroid*). Biovolume (cylinder) uses a simple cylindrical volume calculation (volume = $\pi$ radius$^2$ height) with *geodesic length* as height and half the *geodesic thickness* as radius. Biovolume (sphere) uses a simple spherical volume calculation (volume = 4/3 $\pi$ radius$^3$) using half the ABD as radius. Biovolume (p. spheroid) uses a prolate spheroid volume calculation (volume = 4/3 $\pi$ width$^2$ length) where width is the minor axis of the *Legendre ellipse* and length is the major axis of the Legendre ellipse. Eight recent papers have taken advantage of these newer shape-based biovolume FlowCam outputs, assigning different output types based on the shape of classified cells. While this appears logical on the surface, these (and many other) *VisualSpreadsheet* outputs inherently contain multiple and cascading levels of error from particle property estimation to shape assumption and biovolume calculation. With squared and cubed values in these formulae, any errors or improper selection of outputs for cells will be compounded, and so their use should be carefully considered.

To highlight the effects of measurement output selection on findings, the following two case studies were conducted as examples to quantify the impact of measurement output selection (ABD compared to ESD, Case Study 2), and to illustrate why automated outputs should be approached with caution (with biovolume (cylinder) as an example, Case Study 3).

### *Case study 2*

Natural mixed phytoplankton samples collected from the Swan-Canning Estuary (Perth, Western Australia) were stained with Lugol's iodine solution, pre-filtered to exclude particles > 50 $\mu$m, concentrated $\times$20 by sedimentation, and processed through the aforementioned FlowCam (see Case Study 1) in auto-image mode, again using a 20$\times$ objective and standard (FV50) 50 $\mu$m flow cell (full methods details provided in Supporting Information Appendix C). Output images from three sampling sites spanning saline, brackish, and freshwater parts of the estuary (12,287, 13,385, and 13,734 images, respectively) were manually classified to exclude non-phytoplankton images within *VisualSpreadsheet* (Version 4.12.3) and size measurements (ABD and ESD) were exported. A Spearman's correlation and Wilcoxon matched-pair signed rank test were performed with IBM SPSS Statistics (Version 24).

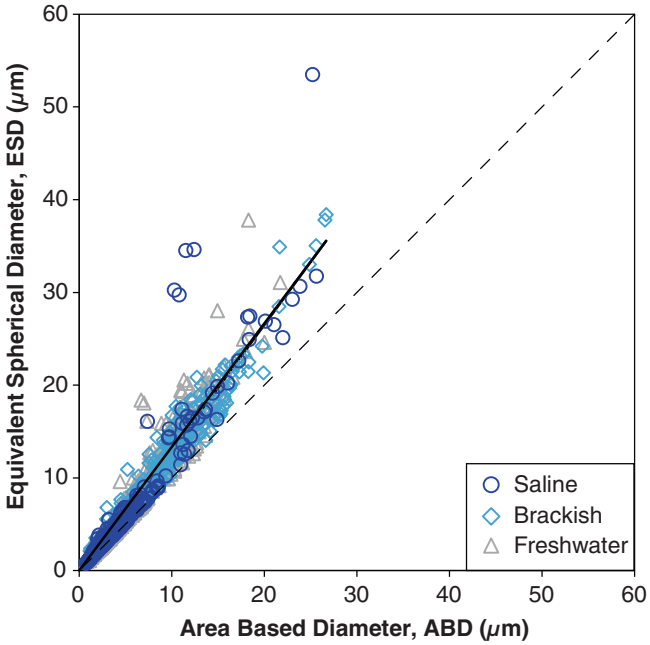


**Fig. 2.** Automated FlowCam measurement outputs for three mixed natural phytoplankton samples, illustrating the effect of the selection of either ABD or ESD measurements on outputs. Solid line is linear trendline, dotted line represents 1 : 1 line.

While a significant strong positive linear correlation was evident between ABD and ESD measurement outputs ($r_{1804} = 0.99$, $p < 0.001$, Fig. 2), the mean ESD outputs were significantly higher (6.73 $\pm$ 0.13 $\mu$m) than ABD outputs (5.43 $\pm$ 0.09 $\mu$m, $Z = 36.80$, $p < 0.001$). Most divergences between ABD and ESD measurements were for particles greater than 20 $\mu$m (Fig. 2), likely reflecting the mostly circular shapes of smaller cells and more complex shapes of larger cells within the samples. These findings further highlight the necessity of providing justification for the selection of FlowCam measurement output parameters and their calibration to microscopy or other means of measurement.

### *Case study 3*

Image outputs from the previous case study were manually sorted in *VisualSpreadsheet* (Version 4.12.3) to isolate 60 clear images of centric diatoms (*Cyclotella* spp. or *Thalassiosira* spp.), with 30 in girdle-view and 30 in valve-view (see

Supporting Information Appendix D for images and a more detailed outline of the following investigations). Measurement outputs for these 60 images (*area* [*filled*], *biovolume* [*cylinder*], ESD, *feret length* [FL], *feret width* [FW], *geodesic length* [GL], *geodesic thickness* [GT], and *perimeter*) were exported and compared in Microsoft Excel. These values were used to investigate the application of the automated biovolume (cylinder) output to represent diatom images, as is increasingly reported in published studies (8 studies in the last 4 yr). Although centric diatoms are basically a cylinder shape, there are two key issues with this output: it is automatically derived from the already automatically derived geodesic length and thickness metrics and it is a three-dimensional volume formula that is automatically applied to automatically collected two-dimensional images.

The FlowCam manual states that the geodesic length and thickness outputs are derived by modeling the particle as a rectangle which matches both the area (filled) and perimeter measures (which are both directly computed from the pixels of the image), to simultaneously solve the equations (area [filled] = GL × GT) and (perimeter = 2 × [GL + GT]). To visualize this process, you would start with a square with the same area as the particle and then flatten/elongate this into a rectangle until it has the same perimeter as the particle, with the length and width of this rectangle being the geodesic length and thickness. As a circle has a lower perimeter-to-area ratio than a square, geodesics cannot be computed for a circle, but *VisualSpreadsheet* outputs a geodesic length and thickness for all images, including all 30 circular valve-view images (see Supporting Information Appendix D for example outputs). For the 60 images considered, 2 × (GL + GT) did equal perimeter, but GL × GT did not equal the area (filled) output for any examples. Using the provided root metrics (area [filled] and perimeter) and the quadratic equation to solve the stated simultaneous equations we were able to produce GL and GT values that meet the stated rules, but do not match the *VisualSpreadsheet* GL and GT outputs (see Supporting Information Appendix D for values). This indicates that there is an error with the inbuilt automated calculation of FlowCam geodesics, and their use (and outputs derived from them) should be approached with caution.

The 30 girdle-view diatom images are essentially rectangles representing the side-on view of squat cylinders whose length would be the cylinder diameter and width would be the cylinder height for a cylindrical volume calculation (where volume = $\pi$ [diameter/2]$^2$ height). The FlowCam automated biovolume (cylinder) output uses GT to represent diameter and GL to represent height, which is the reverse of what would be appropriate for the 30 cells considered here (diameter and height are swapped). In addition to the described fault in geodesics derivation, this automatically applied formula is not appropriate for these diatom cells—an issue that is compounded by the cubing in the formula. A cylindrical volume could be manually calculated from FlowCam outputs of girdle-view images by using the more reliable FL for diameter and FW for height, although this would need to be flipped for tall/narrow diatoms (Spaulding et al. 2012).

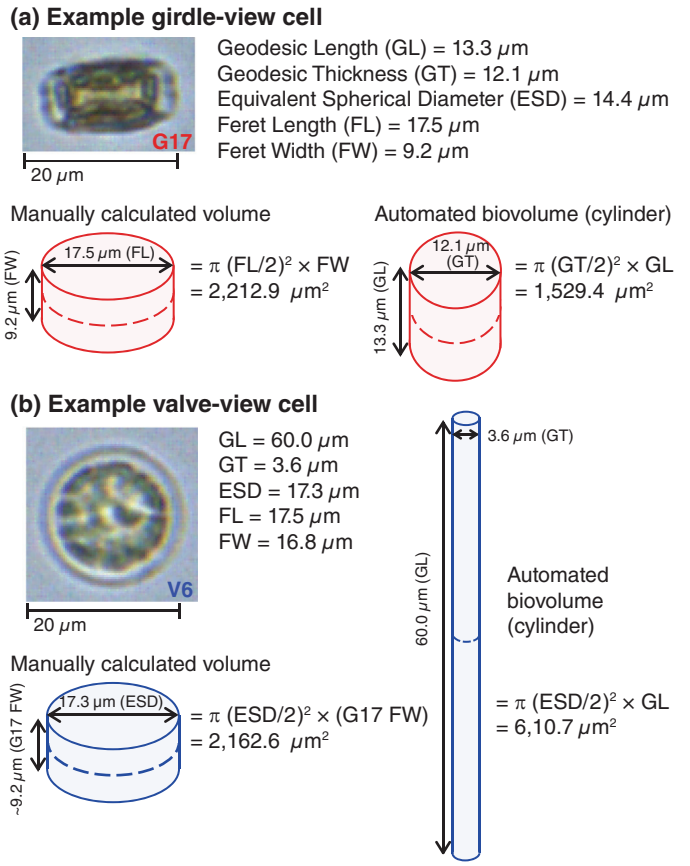


**Fig. 3.** Manual and automated cylindrical volume estimates for an example (**a**) girdle-view cell (G17), and (**b**) valve-view cell (V6). Diameter was represented by ESD (rather than ABD) for the valve-view cell because the cell has no large protrusions but does include translucent inner components. The feret width of girdle-view cell G17 was used to approximate height for valve-view cell V6, as both cells have a similar feret length (approximate diameter) and height cannot be directly measured for valve-view images.

Cylindrical volume cannot be calculated based on valve-view images of centric diatoms (the circular top view of the cylinder) alone, as the cylinder height cannot be extracted. The FlowCam automated biovolume (cylinder) output does not differentiate cell orientation, and so again uses GL and GT as inputs. The automated biovolume (cylinder) output is not appropriate for any valve-view diatom images for three reasons; (i) FlowCam geodesics are incorrect, (ii) geodesics cannot be calculated for circles, and (iii) no automated value can represent cylinder height. A cylindrical volume could be manually calculated for valve-view images by using ABD or ESD for diameter and approximating height by manually determining a diameter-to-height ratio based on sufficient girdle-view images of the same species (our sample size of 30 was not large enough for this, see Supporting Information Appendix D).

To visualize these issues with the automated biovolume (cylinder) output, an example girdle-view and valve-view image is shown in Fig. 3, along with diagrams to approximate the correct and automated diameter, height, and volume measures. These examples clearly highlight that due to the complexities of calculating measures based on two-dimensional images, automated outputs can exhibit marked errors. Given this finding, the veracity of the 10 studies that used FlowCam geodesic length, geodesic width or biovolume (cylinder) outputs is brought into question, especially where those findings were compared to previous data collected using traditional manual microscopy techniques (Krause and Lomas 2020). It is vital that researchers carefully consider which automated outputs they make use of and take the time to check that they accurately represent the features they are estimating for their specific cells.

## Discussion

This study has evaluated the efficacy of methods reporting across the 116 peer reviewed studies published between 2017 and 2020 that used a FlowCam for phytoplankton analysis. We identified a variety of method details that were poorly documented, despite their potential to significantly affect study outcomes. These include failures to provide sufficient details for methods used to collect and prepare phytoplankton samples for FlowCam analysis (78% of studies missing critical details), the FlowCam technical specifications (99%) and specific settings and hardware employed (94%), the approaches used for sorting of images (60%) and use of cell measurement estimates (84%). No single study reported their methods in sufficient detail to enable the study to be reproduced by independent researchers. The possibility of independent replication of study findings is crucial for validation and comparison of findings (Baker 2016). Comprehensive description of the methods used to collect and process FlowCam images also facilitates scientific progress, allowing future users to build on existing studies rather than starting from first principles in each case. By identifying a specific list of methods details that can impact FlowCam phytoplankton study findings, we contribute one step toward better scientific methods reporting in the future.

The identified critical shortcomings in the reporting of FlowCam methods make the findings of most published studies difficult to interpret and compare, hampering rigorous evaluation of the capabilities of the FlowCam and resulting in lower confidence in the findings presented by such studies. For example, Park et al. (2019*a*) presented and evaluated a method for counting *Microcystis* colonies using FlowCam measurement outputs and a novel model algorithm to convert these size measures to cell counts, concluding that their technique can be used for rapid and unbiased analysis of algal blooms (when compared to traditional manual microscopy). However, key method details are missing from this study including the version of *VisualSpreadsheet* used, the sample preservation methods, the FlowCam sample processing methods, and most crucially which of the 47 available FlowCam measurement outputs were used for their technique. Because of these omissions it is not possible to either evaluate the rigor of or make use of the proposed method.

Readers unfamiliar with the intricacies of the FlowCam are unlikely to understand from the methods presented that most papers do not make use of the widely advertised auto-classification capabilities of the device. The statement that classifications were conducted "using VisualSpreadsheet software," employed by many papers (Bergkemper and Weisse 2017; Fileman et al. 2017; Wirth et al. 2019), is insufficient given that this software can be used solely for processing samples through the FlowCam, for auto-classifications of images produced by the FlowCam or simply as an image-viewing interface for manual sorting of images. Furthermore, some papers have provided detailed explanation in their methods section of the creation of image libraries for the apparent purpose of auto-classification, only to reveal later in the discussion section that the image library was not used or tested in the study (Park et al. 2019*a*). It is therefore unsurprising that even experienced FlowCam users are confused about its capabilities. For example, Kydd et al. (2018) referenced Álvarez et al. (2014) as evidence of the FlowCam auto-classification capabilities, yet the latter study did not test this. Jyothibabu et al. (2018*b*) stated that the FlowCam imaged "all particles present in the sample," although some particles will be out of the plane of focus or will fall through between image captures even with FOV flow cells (Camoying and Yñiguez 2016). Similarly, Cabanelas et al. (2016) stated that the FlowCam provides the "actual cell diameter" of cells; the FlowCam provides three different measures of cell diameter, none of which could be definitively taken as the "actual" diameter in all contexts.

Automated devices like the FlowCam can rapidly produce a large number of potentially valuable outputs, but users must be careful not to use these blindly. We have outlined how automated FlowCam outputs for cell density, taxonomic composition, and cell size need to be deliberately chosen, calibrated, and validated for the specific sample being analyzed. As we have shown with the shape-based biovolume outputs, similar-sounding outputs are not necessarily computed in similar ways and are not necessarily accurate or suitable for use with all images. We have demonstrated that FlowCam geodesic measures and their derivatives are incorrectly calculated, bringing into question the validity of studies making use of these outputs. There is clearly confusion regarding the derivation of these values by those making use of them. For example, Greer et al. (2020) state that "FlowCAM software provided estimates of biovolume ($\mu m^3$) for each phytoplankton group based on a projected two-dimensional shape (e.g., cylinder, prolate spheroid, or sphere) of each particle using the ESD," although none of these estimates are based on the ESD. Similarly, Yang et al. (2017*a*,*b*) confuses the computation of ABD and ESD, which we have shown to be distinctly different,

stating "the volume of each cell was estimated using the ABD algorithm, which equates the volume estimated from an equivalent spherical diameter."

There are important implications for the identified issues with FlowCam methods and the observed misunderstandings by FlowCam users. If waterbody managers tasked with making decisions on closing or reopening waterbodies and fisheries due to the presence of harmful algae are basing their decisions on FlowCam data, inaccurate cell identifications (caused by reduced image quality), inaccurate cell densities (caused by imbalanced sample processing techniques) or inaccurate cell biovolumes (caused by improper selection of measurement outputs) can have significant health and economic risks. There can be major implications for study outcomes in cases where FlowCam data collected with questionable methods are compared to other studies or inserted into large existing datasets, such as for the analysis of long-term ecological trends or for quantifying blue carbon sequestration in the context of greenhouse gas reduction (Dunne et al. 2007; Lovelock and Duarte 2019).

As an example, Lomas et al. (2019) and Krause and Lomas (2020) both used the FlowCam automated biovolume (cylinder) measure to represent biovolume of mixed diatom samples when proposing and validating a new method for calculating cold-water diatom elemental density, an important measure used to reflect diatom standing stocks and carbon flux, and for predicting the influences of climate change. Lomas et al. (2019) present the new cold-water diatom allometry calculation based on FlowCam biovolume (cylinder) outputs, while Krause and Lomas (2020) test the calculation on additional FlowCam biovolume (cylinder) outputs and then also compare these findings to those of several prior studies (not using FlowCam) that relied on existing temperate diatom allometry calculations, concluding that the new method is different (with diatom contributions significantly increased) but superior. We have shown (in Case Study 3) that this FlowCam output is calculated incorrectly and produces either over- or under-estimates of biovolume depending on diatom orientation. Lomas et al. (2019) do not describe any FlowCam image sorting, while Krause and Lomas (2020) specifically state that images were manually sorted to exclude empty frustules, but do not mention cell orientation. Lomas et al. (2019) state that their FlowCam biovolume (cylinder) estimates compared favorably to manual microscopic quantification (no data are provided), but we know that this measure is incorrect, especially for unsorted cell orientations. Partially based on faulty FlowCam outputs, these studies claim that previous non-FlowCam studies have systematically underestimated the role of diatoms in polar waters, and suggest future studies should use the new calculations. This example illustrates the wide reach (well beyond other FlowCam users) of the implications for the inappropriate use of FlowCam outputs and insufficient FlowCam methods reporting.

The gaps in methods reporting that we have described here are not unique to FlowCam, digital imaging more broadly, or even aquatic research in general. Within the field of medical research, for example, various reviews have identified similarly widespread deficiencies in the reporting of methods (Meinert et al. 1984; Chan and Altman 2005). In response to these shortcomings, researchers in these fields have developed clear standards for reporting medical research, in the form of explicit guidelines such as the Consolidated Standards of Reporting Trials (CONSORT) for randomized controlled trials (Altman 1996). Subsequent reviews have established that articles that follow the established CONSORT guidelines report key methods details more thoroughly (Plint et al. 2006; Kane et al. 2007; Turner et al. 2012). Standardized reporting guidelines have been developed for a range of medical techniques, including observational studies in epidemiology (Von Elm et al. 2007), biomedical studies involving animals (Kilkenny et al. 2010), clinical trial protocols (Chan et al. 2013) and functional Magnetic Resonance Imaging (MRI) studies (Carp 2012). This proven success of standardized reporting guidelines in the medical field indicates that reporting guidelines would also be beneficial to other fields and technological platforms, including digital imaging.

Rigorous reporting of plankton imaging methods is even more vital in light of recent advances in the realms of artificial intelligence and deep learning, which are an important next step for dealing with the data produced by devices like the FlowCam (González et al. 2017). To be able to assist with plankton analysis, these fields require large datasets for algorithm development and validation, but these datasets need to be standardized with critical image collection methods fully preserved. A recent working group produced a technical manual specifically setting out a protocol for submitting appropriate plankton image datasets to global open-access data repositories such as SeaBASS, OBIS, and EcoTaxa, including the details required when describing the methods for image collection (Neeley et al. 2021). These include descriptions of the instrument used, key instrument settings employed, image post-processing methods and metrics included. However, those guidelines are not specific to any plankton imaging device, and our paper serves as a guide to which details are necessary to include for the FlowCam specifically.

Due to the proliferation of new scientific technologies over recent decades, no editor or reviewer can be expected to understand the intricacies and methods reporting requirements of each new device. The responsibility to report methods in sufficient detail ultimately falls to the authors, and users familiar with each technology should aim to produce specific but clear reporting guidelines to assist authors with meeting this responsibility, as we have done here. Crucially, most journals now allow for the inclusion of extensive online Supporting Information, in which methods can be described in full detail without compromising the clarity of manuscripts. Where this option is not available, authors can take advantage of alternative means for providing access to supporting documents, such as the Open Science Framework [OpenScienceFramework.org].

## Comments and recommendations

Based on the findings of the present study, we have identified a key set of characteristics that should be reported by studies using the FlowCam to image phytoplankton, to ensure that future studies allow for the possibility of independent replication and to facilitate scientific progress in this field:

1. *FlowCam technical specifications*: Full FlowCam model number and machine serial number, camera type (color or monochrome and resolution), pump type (peristaltic, syringe or ALH), and the details of any upgrades to the machine.
2. *Sample details*: Cell concentration, preservation methods, dilution or concentration details, pre-filtration details, and sample particle composition (presence of detritus, etc.).
3. *FlowCam setup details*: Flow cell sizes and types (standard or FOV), objectives used for each flow cell, image collection mode (auto-image, scatter-triggered or fluorescence-triggered, including wavelengths), framerate, flow rate, sample volume imaged, number of images collected, any other relevant context settings (shutter speed, gain, intensity, size filters), and the methods used to determine cell density.
4. *Image sorting details*: Manual, automated or combination of automated and manual, and which software used for any automated sorting. Details of inclusion/exclusion criteria for sorting. If *VisualSpreadsheet* or *Classifier Advanced*; image library description and sizes, choices of particle property settings and all other settings, and an evaluation of the accuracy of auto-classifications.
5. *Measurement outputs (if used)*: Measurement type(s) used, with a justification with careful consideration for this choice for the cell-types being analyzed and/or calibration to traditional forms of measurement.

An example supplementary information template is provided (Supporting Information Appendix E), which should facilitate researchers to provide the necessary detail without cluttering their methods sections. This guideline could be easily adapted for other FlowCam uses, and for future additions to the FlowCam range. In addition, the principles applied here can be adapted to produce similar guidelines for other devices, from other digital imaging devices to any automated or semi-automated technologies.

Adequate methods reporting is essential for scientific progress and to ensure the rigor, comparability, and reproducibility of published scientific outputs. We have documented widespread deficiencies in the reporting of FlowCam methods for phytoplankton analysis and have shown via case studies that these may have significant implications for the reproducibility and interpretation of published research. Researchers in this field and others should aim to rigorously report all relevant method details for future work, and we hope that our findings and recommendations will facilitate this.

## References


Aaron, J., and T. Chew. 2021. A guide to accurate reporting in digital imaging processing – Can anyone reproduce your quantitative analysis? J. Cell Biol. **134**: jcs254151. doi:10.1242/jcs.254151

Altman, D. G. 1996. Better reporting of randomised controlled trials: The CONSORT statement. Br. Med. J. **313**: 570–571. doi:10.1136/bmj.313.7057.570

Álvarez, E., Á. López-Urrutia, E. Nogueira, and S. Fraga. 2011. How to effectively sample the plankton size spectrum? A case study using FlowCAM. J. Plankton Res. **33**: 1119–1133. doi:10.1093/plankt/fbr012

Álvarez, E., Á. López-Urrutia, and E. Nogueira. 2012. Improvement of plankton biovolume estimates derived from image-based automatic sampling devices: Application to FlowCAM. J. Plankton Res. **34**: 454–469. doi:10.1093/plankt/fbs017

Álvarez, E., M. Moyano, Á. López-Urrutia, E. Nogueira, and R. Scharek. 2014. Routine determination of plankton community composition and size structure: A comparison between FlowCAM and light microscopy. J. Plankton Res. **36**: 170–184. doi:10.1093/plankt/fbt069

Álvarez, E., E. Nogueira, and Á. López-Urrutia. 2017. In vivo single-cell fluorescence and size scaling of phytoplankton chlorophyll content. Appl. Environ. Microbiol. **83**: e03317-16. doi:10.1128/AEM.03317-16

Anderson, S. R., Q. P. Diou-Cass, and E. L. Harvey. 2018. Short-term estimates of phytoplankton growth and mortality in a tidal estuary. Limnol. Oceanogr. **63**: 2411–2422. doi:10.1002/lno.10948

Anderson, S. R., and E. L. Harvey. 2019. Seasonal variability and drivers of microzooplankton grazing and phytoplankton growth in a subtropical stuary. Front. Mar. Sci. **6**: 174. doi:10.3389/fmars.2019.00174

Arrigo, K. R., and others. 2017. Early spring phytoplankton dynamics in the Western Antarctic Peninsula. J. Geophys. Res. Oceans **122**: 9350–9369. doi:10.1002/2017JC013281

Babin, M., and others. 2005. New approaches and technologies for observing harmful algal blooms. Oceanography **18**: 210–227. doi:10.5670/oceanog.2005.55

Baer, S. E., S. Rauschenberg, C. A. Garcia, N. S. Garcia, A. C. Martiny, B. S. Twining, and M. W. Lomas. 2019. Carbon and nitrogen productivity during spring in the oligotrophic Indian Ocean along the GO-SHIP IO9N transect. Deep Sea. Res. Pt. II **161**: 81–91. doi:10.1016/j.dsr2.2018.11.008

Baker, M. 2016. 1,500 scientists lift the lid on reproducibility. Nature **533**: 452–454. doi:10.1038/533452a

Bartual, A., and others. 2020. Types and distribution of bioactive polyunsaturated aldehydes in a gradient from mesotrophic to oligotrophic waters in the Alborán Sea (Western Mediterranean). Mar. Drugs **18**: 159. doi:10.3390/md18030159

Bayer, M. M., S. J. M. Droop, and D. G. Mann. 2001. Digital microscopy in phycological research, with special reference to microalgae. Phycol. Res. **49**: 263–274. doi:10.1046/j.1440-1835.2001.00246.x

Benfield, M. C., and others. 2007. RAPID: Research on automated plankton identification. Oceanography **20**: 172–187. doi:10.5670/oceanog.2007.63

Bergkemper, V., and T. Weisse. 2017. Phytoplankton response to the summer 2015 heat wave—a case study from prealpine Lake Mondsee, Austria. Inland Waters **7**: 88–99. doi:10.1080/20442041.2017.1294352

Bergkemper, V., and T. Weisse. 2018. Do current European lake monitoring programmes reliably estimate phytoplankton community changes? Hydrobiologia **824**: 143–162. doi:10.1007/s10750-017-3426-6

Bernhardt, J. R., J. M. Sunday, and M. I. O'Connor. 2018a. Metabolic theory and the temperature-size rule explain the temperature dependence of population carrying capacity. Am. Nat. **192**: 687–697. doi:10.1086/700114

Bernhardt, J. R., J. M. Sunday, P. L. Thompson, and M. I. O'Connor. 2018b. Nonlinear averaging of thermal experience predicts population growth rates in a thermally variable environment. Proc. Roy. Soc. B Biol. Sci. **285**: 20181076. doi:10.1098/rspb.2018.1076

Beutler, M. 2003. Spectral fluorescence of chlorophyll and phycobilins as an in-situ tool of phytoplankton analysis-models, algorithms and instruments. PhD thesis. Christian-Albrechts Universität Kiel. hdl.handle.net/11858/00-001M-0000-000F-DBE8-F

Bishop, I. W., and S. A. Spaulding. 2017. Life cycle size dynamics in *Didymosphenia geminata* (Bacillariophyceae). J. Phycol. **53**: 652–663. doi:10.1111/jpy.12528

Black, J. G., J. S. Stark, G. J. Johnstone, A. McMinn, P. Boyd, J. McKinlay, S. Wootherspoon, and J. W. Runcie. 2019. In-situ behavioural and physiological responses of Antarctic microphytobenthos to ocean acidification. Sci. Rep. **9**: 1–13. doi:10.1038/s41598-018-36233-2

Borja, A., and others. 2008. Overview of integrative tools and methods in assessing ecological integrity in estuarine and coastal systems worldwide. Mar. Pollut. Bull. **56**: 1519–1537. doi:10.1016/j.marpolbul.2008.07.005

Briggs, N., K. Guðmundsson, I. Cetinić, E. D'Asaro, E. Rehm, C. Lee, and M. J. Perry. 2018. A multi-method autonomous assessment of primary productivity and export efficiency in the springtime North Atlantic. Biogeosciences **15**: 4515–4532. doi:10.5194/bg-15-4515-2018

Brzezinski, M. A., and others. 2011. Co-limitation of diatoms by iron and silicic acid in the equatorial Pacific. Deep Sea. Res. Pt. II **58**: 493–511. doi:10.1016/j.dsr2.2010.08.005

Buskey, E. J., and C. J. Hyatt. 2006. Use of the FlowCAM for semi-automated recognition and, enumeration of red tide cells (*Karenia brevis*) in natural plankton samples. Harmful Algae **5**: 685–692. doi:10.1016/j.hal.2006.02.003

Cabanelas, I. T. D., M. Van Der Zwart, D. M. Kleinegris, R. H. Wijffels, and M. J. Barbosa. 2016. Sorting cells of the microalga *Chlorococcum littorale* with increased triacylglycerol productivity. Biotechnol. Biofuels **9**: 183. doi:10.1186/s13068-016-0595-x

Calver, M. C., B. Goldman, P. A. Hutchings, and R. T. Kingsford. 2017. Why discrepancies in searching the conservation biology literature matter. Biol. Conserv. **213**: 19–26. doi:10.1016/j.biocon.2017.06.028

Camoying, M. G. 2016. Characterization of the spatial variability of phytoplankton community structure in two key sardine fishery areas in the Phillipines using FlowCAM. Masters Thesis. Univ. of the Phillipines.

Camoying, M. G., and A. T. Yñiguez. 2016. FlowCAM optimization: Attaining good quality images for higher taxonomic classification resolution of natural phytoplankton samples. Limnol. Oceanogr. Methods **14**: 305–314. doi:10.1002/lom3.10090

Carp, J. 2012. The secret lives of experiments: Methods reporting in the fMRI literature. Neuroimage **63**: 289–300. doi:10.1016/j.neuroimage.2012.07.004

Casas-Monroy, O., H. Rajakaruna, and S. A. Bailey. 2020. Improving estimation of phytoplankton abundance and distribution in ballast water discharges. J. Appl. Phycol. **32**: 1–15. doi:10.1007/s10811-019-02034-x

Chaffin, J. D., D. D. Kane, K. Stanislawczyk, and E. M. Parker. 2018a. Accuracy of data buoys for measurement of cyanobacteria, chlorophyll, and turbidity in a large lake (Lake Erie, North America): Implications for estimation of cyanobacterial bloom parameters from water quality sonde measurements. Environ. Sci. Pollut. R. **25**: 25175–25189. doi:10.1007/s11356-018-2612-z

Chaffin, J. D., T. W. Davis, D. J. Smith, M. M. Baer, and G. J. Dick. 2018b. Interactions between nitrogen form, loading rate, and light intensity on *Microcystis* and *Planktothrix* growth and microcystin production. Harmful Algae **73**: 84–97. doi:10.1016/j.hal.2018.02.001

Chaffin, J. D., K. Stanislawczyk, D. D. Kane, and M. M. Lambrix. 2020a. Nutrient addition effects on chlorophyll a, phytoplankton biomass, and heterocyte formation in Lake Erie's central basin during 2014–2017: Insights into diazotrophic blooms in high nitrogen water. Freshw. Biol. **65**: 2154–2168. doi:10.1007/s11356-018-2612-z

Chaffin, J. D., D. D. Kane, and A. Johnson. 2020b. Effectiveness of a fixed-depth sensor deployed from a buoy to estimate water-column cyanobacterial biomass depends on wind speed. J. Environ. Sci. **93**: 23–29. doi:10.1016/j.jes.2020.03.003

Chan, A.-W., and D. G. Altman. 2005. Epidemiology and reporting of randomised trials published in PubMed journals. Lancet **365**: 1159–1162. doi:10.1016/S0140-6736(05)71879-1

Chan, A.-W., and others. 2013. SPIRIT 2013 statement: Defining standard protocol items for clinical trials. Ann. Intern.

Med. **158**: 200–207. doi:10.7326/0003-4819-158-3-201302050-00583

Chaplin, C. C., M. Tabor, I. A. Marquez, K. Maiti, and J. W. Krause. 2019. Resuscitation of microalgae from Mississippi River plume sediments. Gulf Caribb. Res. **30**: SC38-SC41. doi:10.18785/gcr.3001.15

Clayton, S., L. Gibala-Smith, K. Mogatas, C. Flores-Vargas, K. Marciniak, M. Wigginton, and M. R. Mulholland. 2022. Imaging technologies build capacity and accessibility in phytoplankton species identification expertise for research and monitoring: Lessons learned during the COVID-19 pandemic. Front. Microbiol. **13**: 823109. doi:10.3389/fmicb.2022.823109

Coello-Camba, A., M. Llabrés, C. M. Duarte, and S. Agusti. 2017. Zooplankton excretion metabolites stimulate Southern Ocean phytoplankton growth. Polar Biol. **40**: 2035–2045. doi:10.1007/s00300-017-2123-2

Corcoran, A. A., M. Seger, R. Niu, N. Nirmalakhandan, P. J. Lammers, F. O. Holguin, and W. J. Boeing. 2019. Evidence for induced allelopathy in an isolate of *Coelastrella* following co-culture with *Chlorella sorokiniana*. Algal Res. **41**: 101535. doi:10.1016/j.algal.2019.101535

Cornwell, L. E., and others. 2020. Resilience of the copepod Oithona similis to climatic variability: Egg production, mortality, and vertical habitat partitioning. Front. Mar. Sci. **7**: 29. doi:10.3389/fmars.2020.00029

Cosgrove, J., and M. Borowitzka. 2006. Applying pulse amplitude modulation (PAM) fluorometry to microalgae suspensions: Stirring potentially impacts fluorescence. Photosynth. Res. **88**: 343–350. doi:10.1007/s11120-006-9063-y

Cosgrove, J., and M. A. Borowitzka. 2010. Chlorophyll fluorescence terminology: An introduction, p. 1–17. *In* D. J. Suggett, O. Prášil, and M. A. Borowitzka [eds.], Chlorophyll *a* fluorescence in aquatic sciences: Methods and applications. Springer.

De-los-Ríos-Mérida, J., A. Reul, M. Muñoz, S. Arijo, S. Tapia-Paniagua, M. Rendón-Martos, and F. Guerrero. 2017. How efficient are semi-natural ponds in assimilating wastewater effluents? Application to Fuente de Piedra Ramsar, Mediterranean salt lake (south of Spain). Water **9**: 600. doi:10.3390/w9080600

do Rosario Gomes, H., K. McKee, A. Mile, S. Thandapu, K. Al-Hashmi, X. Jiang, and J. I. Goes. 2018. Influence of light availability and prey type on the growth and photophysiological rates of the mixotroph *Noctiluca scintillans*. Front. Mar. Sci. **5**: 374. doi:10.3389/fmars.2018.00374

Dunne, J. P., J. L. Sarmiento, and A. Gnanadesikan. 2007. A synthesis of global particle export from the surface ocean and cycling through the ocean interior and on the seafloor. Global Biogeochem. Cycl. **21**: GB4006. doi:10.1029/2006GB002907

Edwards, M., D. Broughton, R. Camp, G. Graham, P. Helaouet, and R. Stern. 2017. AtlantOS plankton report: based on observations from the Continuous Plankton Recorder Survey. Sir Alister Hardy Foundation for Ocean Science. doi:10.3289/AtlantOS_D2.1

Falkowski, P. G., and M. J. Oliver. 2007. Mix and match: How climate selects phytoplankton. Nat. Rev. Microbiol. **5**: 813–819. doi:10.1038/nrmicro1751

Farrow, C. R., J. D. Ackerman, R. E. Smith, and D. Snider. 2020. Riverine transport and nutrient inputs affect phytoplankton communities in a coastal embayment. Freshw. Biol. **65**: 289–303. doi:10.1111/fwb.13421

Feng, B., C. Wang, X. Wu, C. Tian, M. Zhang, Y. Tian, and B. Xiao. 2019a. Spatiotemporal dynamics of cell abundance, colony size and intracellular toxin concentrations of pelagic and benthic *Microcystis* in Lake Caohai, China. J. Environ. Sci. (China) **84**: 184–196. doi:10.1016/j.jes.2019.05.010

Feng, B., C. Wang, X. Wu, C. Tian, Y. Tian, and B. Xiao. 2019b. Involvement of microcystins, colony size and photosynthetic activity in the benthic recruitment of *Microcystis*. J. Appl. Phycol. **31**: 223–233. doi:10.1007/s10811-018-1508-0

Fileman, E. S., D. A. White, R. A. Harmer, Ü. Aytan, G. A. Tarran, T. Smyth, and A. Atkinson. 2017. Stress of life at the ocean's surface: Latitudinal patterns of UV sunscreens in plankton across the Atlantic. Prog. Oceanogr. **158**: 171–184. doi:10.1016/j.pocean.2017.01.001

Franzè, G., and P. J. Lavrentyev. 2017. Microbial food web structure and dynamics across a natural temperature gradient in a productive polar shelf system. Mar. Ecol. Prog. Ser. **569**: 89–102. doi:10.3354/meps12072

Fung, V., and J. D. Ackerman. 2020. The effects of river algae and pore water flow on the feeding of juvenile mussels. Eur. J. Vasc. Endovasc. Surg. **125**: e2019JG005302. doi:10.1029/2019JG005302

Giling, D. P., and others. 2017. Thermocline deepening boosts ecosystem metabolism: Evidence from a large-scale lake enclosure experiment simulating a summer storm. Glob. Change Biol. **23**: 1448–1462. doi:10.1111/gcb.13512

Goldberg, C. S., and others. 2016. Critical considerations for the application of environmental DNA methods to detect aquatic species. Methods Ecol. Evol. **7**: 1299–1307. doi:10.1111/2041-210X.12595

González, P., E. Álvarez, J. Díez, Á. López-Urrutia, and J. J. del Coz. 2017. Validation methods for plankton image classification systems. Limnol. Oceanogr.: Methods **15**: 221–237. doi:10.1002/lom3.10151

Göritz, A., S. A. Berger, P. Gege, H. P. Grossart, J. C. Nejstgaard, S. Riedel, R. Röttgers, and C. Utschig. 2018. Retrieval of water constituents from hyperspectral in-situ measurements under variable cloud cover—a case study at Lake Stechlin (Germany). Remote Sens. (Basel) **10**: 181. doi:10.3390/rs10020181

Goulet, T. L., K. P. Shirur, B. D. Ramsby, and R. Iglesias-Prieto. 2017. The effects of elevated seawater temperatures on Caribbean gorgonian corals and their algal symbionts,

*Symbiodinium* spp. PLoS One **12**: e0171032. doi:10.1371/journal.pone.0171032

Graham, M., J. Cook, J. Graydon, D. Kinniburgh, H. Nelson, S. Pilieci, and R. Vinebrooke. 2018. High-resolution imaging particle analysis of freshwater cyanobacterial blooms. Limnol. Oceanogr.: Methods **16**: 669–679. doi:10.1002/lom3.10274

Greer, A. T., and others. 2018. Functioning of coastal river-dominated ecosystems and implications for oil spill response: From observations to mechanisms and models. Oceanography **31**: 90–103. doi:10.5670/oceanog.2018.302

Greer, A. T., and others. 2020. Contrasting fine-scale distributional patterns of zooplankton driven by the formation of a diatom-dominated thin layer. Limnol. Oceanogr. **65**: 2236–2258. doi:10.1002/lno.11450

Gyi, K. K., T. Omura, R. Nakamura, and Y. Tanaka. 2019. High-resolution observations on fine-scale spatial and temporal heterogeneity of phytoplankton communities using flowcam. Mer **57**: 73–87. doi:10.32211/lamer.57.3-4_73

Hallett, C. S., F. Valesini, and M. Elliott. 2016. A review of Australian approaches for monitoring, assessing and reporting estuarine condition: I. International context and evaluation criteria. Environ. Sci. Policy **66**: 260–269. doi:10.1016/j.envsci.2016.07.014

Harvey, E. L., S. R. Anderson, Q. Diou-Cass, and P. I. Duffy. 2020. Assessing the temporal variability and drivers of transparent exopolymer particle concentrations and production rates in a subtropical estuary. Estuar. Coasts **1-10**: 1010–1019. doi:10.1007/s12237-020-00847-5

Hasberg, A. K., and others. 2019. Modern sedimentation processes in Lake Towuti, Indonesia, revealed by the composition of surface sediments. Sedimentology **66**: 675–698. doi:10.1111/sed.12503

Hassett, W., S. M. Bollens, T. D. Counihan, G. Rollwagen-Bollens, J. Zimmerman, S. Katz, and J. Emerson. 2017. Veligers of the invasive Asian clam Corbicula fluminea in the Columbia River Basin: Broadscale distribution, abundance, and ecological associations. Lake Reservoir Manag. **33**: 234–248. doi:10.1080/10402381.2017.1294218

Heddleston, J. M., J. S. Aaron, S. Khuon, and T. Chew. 2021. A guide to accurate reporting in digital image acquisition—can anyone replicate your microscopy data? J. Cell Biol. **134**: jcs254144. doi:10.1242/jcs.254144

Hillebrand, H., C. D. Dürselen, D. Kirschtel, U. Pollingher, and T. Zohary. 1999. Biovolume calculation for pelagic and benthic microalgae. J. Phycol. **35**: 403–424. doi:10.1046/j.1529-8817.1999.3520403.x

Hinners, J., A. Kremp, and I. Hense. 2017. Evolution in temperature-dependent phytoplankton traits revealed from a sediment archive: Do reaction norms tell the whole story? Proc. Biol. Sci. **284**: 20171888. doi:10.1098/rspb.2017.1888

Hötzel, G., and R. Croome. 1999. A phytoplankton methods manual for Australian freshwaters. Land and Water Resources Research and Development Corporation.

Hozumi, A., I. Ostrovsky, A. Sukenik, and H. Gildor. 2020. Turbulence regulation of Microcystis surface scum formation and dispersion during a cyanobacteria bloom event. Inland Waters **10**: 51–70. doi:10.1080/20442041.2019.1637681

Hrycik, A. R., A. Shambaugh, and J. D. Stockwell. 2019. Comparison of FlowCAM and microscope biovolume measurements for a diverse freshwater phytoplankton community. J. Plankton Res. **41**: 849–864. doi:10.1093/plankt/fbz056

Ide, K., K. Takahashi, A. Kuwata, M. Nakamachi, and H. Saito. 2008. A rapid analysis of copepod feeding using FlowCAM. J. Plankton Res. **30**: 275–281. doi:10.1093/plankt/fbm108

Jakobsen, H. H., and J. Carstensen. 2011. FlowCAM: Sizing cells and understanding the impact of size distributions on biovolume of planktonic community structure. Aquat. Microb. Ecol. **65**: 75–87. doi:10.3354/ame01539

Joy-Warren, H. L., and others. 2019. Light is the primary driver of early season phytoplankton production along the Western Antarctic Peninsula. J. Geophys. Res. Oceans **124**: 7375–7399. doi:10.1029/2019JC015295

Jyothibabu, R., N. Arunpandi, L. Jagadeesan, C. Karnan, K. R. Lallu, and P. N. Vinayachandran. 2018a. Response of phytoplankton to heavy cloud cover and turbidity in the northern Bay of Bengal. Sci. Rep. **8**: 11282. doi:10.1038/s41598-018-29586-1

Jyothibabu, R., N. Arunpandi, C. Karnan, L. Jagadeesan, T. Manojkumar, K. Balachandran, and S. Naqvi. 2018b. *Fragilariopsis* sp. bloom causes yellowish-brown waters off Alappuzha, south-central Kerala coast, India, during the mud bank-upwelling phase. Curr. Sci. **115**: 152–159. doi:10.18520/cs/v115/i1/152-159

Jyothibabu, R., C. Karnan, L. Jagadeesan, N. Arunpandi, S. Parthasarathi, and J. A. Konnakkamannil. 2020. Ecological responses of autotrophic microplankton to the eutrophication of the coastal upwelling along the southwest coast of India. Environ. Sci. Pollut. Res. **1–14**: 11401–11414. doi:10.1007/s11356-020-11354-2

Kane, R. L., J. Wang, and J. Garrard. 2007. Reporting in randomized clinical trials improved after adoption of the CONSORT statement. J. Clin. Epidemiol. **60**: 241–249. doi:10.1016/j.jclinepi.2006.06.016

Karnan, C., R. Jyothibabu, T. M. Manoj Kumar, K. K. Balachandran, N. Arunpandi, and L. Jagadeesan. 2017a. Seasonality in autotrophic mesoplankton in a coastal upwelling-mud bank environment along the southwest coast of India and its ecological implications. Cont. Shelf Res. **146**: 1–12. doi:10.1016/j.csr.2017.08.006

Karnan, C., R. Jyothibabu, N. Arunpandi, L. Jagadeesan, K. Muraleedharan, A. Pratihari, K. Balachandran, and S. Naqvi. 2017b. Discriminating the biophysical impacts of coastal upwelling and mud banks along the southwest coast of India. J. Marine Syst. **172**: 24–42. doi:10.1016/j.jmarsys.2017.02.012

Karnan, C., R. Jyothibabu, N. Arunpandi, K. J. Albin, S. Parthasarathi, and S. S. Krishnan. 2020. Response of

microplankton size structure to summer stratification, freshwater influx and coastal upwelling in the southeastern Arabian Sea. Cont. Shelf Res. **193**: 104038. doi:10.1016/j.csr.2019.104038

Kayfetz, K., and W. Kimmerer. 2017. Abiotic and biotic controls on the copepod *Pseudodiaptomus forbesi* in the upper San Francisco Estuary. Mar. Ecol. Prog. Ser. **581**: 85–101. doi:10.3354/meps12294

Keitt, T. H., and E. S. Abelson. 2021. Ecology in the age of automation. Science **373**: 858–859. doi:10.1126/science.abi4692

Kerr, T., J. R. Clark, E. S. Fileman, C. E. Widdicombe, and N. Pugeault. 2020. Collaborative deep learning models to handle class imbalance in FlowCam plankton imagery. IEEE Access **8**: 170013–170032. doi:10.1109/ACCESS.2020.3022242

Keys, M., G. Tilstone, H. S. Findlay, C. E. Widdicombe, and T. Lawson. 2017. Effects of elevated $CO_2$ on phytoplankton community biomass and species composition during a spring *Phaeocystis* spp. bloom in the western English Channel. Harmful Algae **67**: 92–106. doi:10.1016/j.hal.2017.06.005

Kilkenny, C., W. J. Browne, I. C. Cuthill, M. Emerson, and D. G. Altman. 2010. Improving bioscience research reporting: The ARRIVE guidelines for reporting animal research. J. Pharmacol. Pharmacother. **1**: 94–99. doi:10.1371/journal.pbio.1000412

Kimambo, O. N., J. R. Gumbo, T. A. Msagati, and H. Chikoore. 2020. The unusual reddish-bloom appearance in a freshwater fishpond at Kingolwira National Fish Farming Center, Morogoro, Tanzania. Int. J. Environ. **9**: 204–216. doi:10.3126/ije.v9i2.32734

Kofoid, C. A. 1897. On some important sources of error in the plankton method. Science **6**: 829–832 jstor.org/stable/1623279.

Krause, J. W., and M. W. Lomas. 2020. Understanding diatoms' past and future biogeochemical role in high-latitude seas. Geophys. Res. Lett. **47**: e2019GL085602. doi:10.1029/2019GL085602

Kuhlisch, C., J. Althammer, A. F. Sazhin, H. H. Jakobsen, J. C. Nejstgaard, and G. Pohnert. 2020. Metabolomics-derived marker metabolites to characterize *Phaeocystis pouchetii* physiology in natural plankton communities. Sci. Rep. **10**: 1–14. doi:10.1038/s41598-020-77169-w

Kurobe, T., P. W. Lehman, M. E. Haque, T. Sedda, S. Lesmeister, and S. Teh. 2018. Evaluation of water quality during successive severe drought years within *Microcystis* blooms using fish embryo toxicity tests for the San Francisco Estuary, California. Sci. Total Environ. **610**: 1029–1037. doi:10.1016/j.scitotenv.2017.07.267

Kydd, J., H. Rajakaruna, E. Briski, and S. Bailey. 2018. Examination of a high resolution laser optical plankton counter and FlowCAM for measuring plankton concentration and size. J. Sea Res. **133**: 2–10. doi:10.1016/j.seares.2017.01.003

Lampe, R. H., and others. 2018. Divergent gene expression among phytoplankton taxa in response to upwelling. Environ. Microbiol. **20**: 3069–3082. doi:10.1111/1462-2920.14361

Langelier, W. F. 1928. The quantitative estimation of plankton. J. Am. Water Works Assoc. **19**: 408–415. jstor.org/stable/41227566.

Le Bourg, B., V. Cornet-Barthaux, M. Pagano, and J. Blanchot. 2015. FlowCAM as a tool for studying small (80–1000 μm) metazooplankton communities. J. Plankton Res. **37**: 666–670. doi:10.1093/plankt/fbv025

Lehman, P., K. Marr, G. Boyer, S. Acuna, and S. Teh. 2013. Long-term trends and causal factors associated with *Microcystis* abundance and toxicity in San Francisco Estuary and implications for climate change impacts. Hydrobiologia **718**: 141–158. doi:10.1007/s10750-013-1612-8

Lehman, P., T. Kurobe, S. Lesmeister, D. Baxa, A. Tung, and S. J. Teh. 2017. Impacts of the 2014 severe drought on the *Microcystis* bloom in San Francisco Estuary. Harmful Algae **63**: 94–108. doi:10.1016/j.hal.2017.01.011

Lehman, P., T. Kurobe, and S. Teh. 2020. Impact of extreme wet and dry years on the persistence of Microcystis harmful algal blooms in San Francisco Estuary. Quat. Int. **621**: 16–25. doi:10.1016/j.quaint.2019.12.003

Lin, F. S., P. C. Ho, A. R. Sastri, C. C. Chen, G. C. Gong, S. Jan, and C. H. Hsieh. 2019. Resource availability affects temporal variation of phytoplankton size structure in the Kuroshio east of Taiwan. Limnol. Oceanogr. **65**: 236–246. doi:10.1002/lno.11294

Littman, R. A., M. J. van Oppen, and B. L. Willis. 2008. Methods for sampling free-living *Symbiodinium* (zooxanthellae) and their distribution and abundance at Lizard Island (Great Barrier Reef). J. Exp. Mar. Biol. Ecol. **364**: 48–53. doi:10.1016/j.jembe.2008.06.034

Lomas, M. W., S. E. Baer, S. Acton, and J. W. Krause. 2019. Pumped up by the cold: Elemental quotas and stoichiometry of cold-water diatoms. Front. Mar. Sci. **6**: 286. doi:10.3389/fmars.2019.00286

Lombard, F., and others. 2019. Globally consistent quantitative observations of planktonic ecosystems. Front. Mar. Sci. **6**: 196. doi:10.3389/fmars.2019.00196

Loria, K. A., D. McKnight, D. M. Ragar, and P. T. Johnson. 2020. The life aquatic in high relief: Shifts in the physical and biological characteristics of alpine lakes along an elevation gradient in the Rocky Mountains, USA. Aquat. Sci. **82**: 1–16. doi:10.1007/s00027-019-0684-6

Lovelock, C. E., and C. M. Duarte. 2019. Dimensions of blue carbon and emerging perspectives. Biol. Lett. **15**: 20180781. doi:10.1098/rsbl.2018.0781

Magonono, M., P. J. Oberholster, A. Shonhai, S. Makumire, and J. R. Gumbo. 2018. The presence of toxic and non-toxic cyanobacteria in the sediments of the Limpopo River Basin: Implications for human health. Toxins **10**: 269. doi:10.3390/toxins10070269

Marañón, E., P. Cermeño, M. Latasa, and R. D. Tadonléké. 2012. Temperature, resources, and phytoplankton size

structure in the ocean. Limnol. Oceanogr. **57**: 1266–1278. doi:10.4319/lo.2012.57.5.1266

Marañón, E., P. Cermeño, D. C. López-Sandoval, T. Rodríguez-Ramos, C. Sobrino, M. Huete-Ortega, J. M. Blanco, and J. Rodríguez. 2013. Unimodal size scaling of phytoplankton growth and the size dependence of nutrient uptake and use. Ecol. Lett. **16**: 371–379. doi:10.4319/lo.2012.57.5.1266

Marqués, G., T. Pengo, and M. A. Sanders. 2020. Science forum: Imaging methods are vastly underreported in biomedical research. Elife **9**: e55133. doi:10.7554/eLife.55133

Martin, R. M., and others. 2020. Episodic decrease in temperature increases mcy gene transcription and cellular microcystin in continuous cultures of *Microcystis aeruginosa* PCC 7806. Front. Microbiol. **11**: 601864. doi:10.3389/fmicb.2020.601864

Martínez, L. A., J. Mortelmans, N. Dillen, E. Debusschere, and K. Deneudt. 2020. LifeWatch observatory data: Phytoplankton observations in the Belgian Part of the North Sea. Biodivers. Data J. **8**: 57236. doi:10.3897/BDJ.8.e57236

McCauley, E., and J. Kalff. 1981. Empirical relationships between phytoplankton and zooplankton biomass in lakes. Can. J. Fish. Aquat. Sci. **38**: 458–463. doi:10.1139/f81-063

Meinert, C. L., S. Tonascia, and K. Higgins. 1984. Content of reports on clinical trials: A critical review. Control. Clin. Trials **5**: 328–347. doi:10.1016/s0197-2456(84)80013-6

Menden-Deuer, S., E. J. Lessard, and J. Satterberg. 2001. Effect of preservation on dinoflagellate and diatom cell volume and consequences for carbon biomass predictions. Mar. Ecol. Prog. Ser. **222**: 41–50. doi:10.3354/meps222041

Menden-Deuer, S., and others. 2020. Multi-instrument assessment of phytoplankton abundance and cell sizes in monospecific laboratory cultures and whole plankton community composition in the North Atlantic. Front. Mar. Sci. **7**: 254. doi:10.3389/fmars.2020.00254

Milde, A. S., W. B. Richardson, E. A. Strauss, J. H. Larson, J. Vallazza, and B. C. Knights. 2017. Spatial and temporal dynamics of suspended particle characteristics and composition in navigation Pool 19 of the upper Mississippi River. River Res. Appl. **33**: 740–752. doi:10.1002/rra.3131

Mirasbekov, Y., and others. 2021. Semi-automated classification of colonial *Microcystis* by FlowCAM imaging flow cytometry in mesocosm experiment reveals high heterogeneity during seasonal bloom. Sci. Rep. **11**: 9377. doi:10.1038/s41598-021-88661-2

Mistry, R., and J. D. Ackerman. 2018. Flow, flux, and feeding in freshwater mussels. Water Resour. Res. **54**: 7619–7630. doi:10.1029/2018WR023112

Moher, D., A. Liberati, J. Tetzlaff, and D. G. Altman. 2010. Preferred reporting items for systematic reviews and meta-analyses: The PRISMA statement. Int. J. Surg. **8**: 336–341. doi:10.1371/journal.pmed.1000097

Montes, T., E. Guerrero-Feijóo, V. Moreira-Coello, A. Bode, M. Ruiz-Villarreal, B. Mouriño-Carballido, and M. M. Varela. 2020. Vertical zonation of bacterial assemblages attributed to physical stratification during the summer relaxation of the coastal upwelling off Galicia (NW Spain). Estuar. Coast. Shelf Sci. **245**: 106791. doi:10.1016/j.ecss.2020.106791

Munafò, M., and others. 2017. A manifesto for reproducible science. Nat. Hum. Behav. **1**: 0021. doi:10.1038/s41562-016-0021

Muñoz, M., and others. 2017. Fertilization and connectivity in the Garrucha Canyon (SE-Spain) implications for marine spatial planning. Mar. Environ. Res. **126**: 45–68. doi:10.1016/j.marenvres.2017.02.007

Natunen, K., J. Seppälä, R. J. Koivula, and J. Pellinen. 2017. Monitoring cell-specific neutral lipid accumulation in *Phaeodactylum tricornutum* (Bacillariophyceae) with Nile Red staining—a new method for flow CAM. J. Phycol. **53**: 396–404. doi:10.1111/jpy.12504

Neeley, A., and others. 2021. Standards and practices for reporting plankton and other particle observations from images, technical manual. Ocean Carbon & Biogeochemistry Program, Woods Hole Oceanographic Institution. doi:10.1575/1912/27377

Nissimov, J. I., R. Vandzura, C. T. Johns, F. Natale, L. Haramaty, and K. D. Bidle. 2018. Dynamics of transparent exopolymer particle production and aggregation during viral infection of the coccolithophore, *Emiliania huxleyi*. Environ. Microbiol. **20**: 2880–2897. doi:10.1111/1462-2920.14261

Noh, J. H., W. Kim, S. H. Son, J.-H. Ahn, and Y.-J. Park. 2018. Remote quantification of *Cochlodinium polykrikoides* blooms occurring in the East Sea using geostationary ocean color imager (GOCI). Harmful Algae **73**: 129–137. doi:10.1016/j.hal.2018.02.006Get

Nolan, M. P., and B. J. Cardinale. 2019. Species diversity of resident green algae slows the establishment and proliferation of the cyanobacterium *Microcystis aeruginosa*. Limnologica **74**: 23–27. doi:10.1016/j.limno.2018.09.002

Okoli, C., and K. Schabram. 2010. A guide to conducting a systematic literature review of information systems research, v. **10**. SSRN. doi:10.2139/ssrn.1954824

Olenina, I. 2006. Biovolumes and size-classes of phytoplankton in the Baltic Sea. Balt. Sea Environ. Proc. **106**: 1–144.

Omar, R., Z. Ibrahim, Z. Zahid, E. Ismail, I. Hisham, S. I. Omar, and S. Mustafar. 2017. Algae disintegration in raw water at Semberong Barat Dam Johor Malaysia using sonification wave. Res. J. Pharm. Biol. Chem. Sci. **8**: 1931.

Park, J., Y. Kim, M. Kim, and W. H. Lee. 2019a. A novel method for cell counting of *Microcystis* colonies in water resources using a digital imaging flow cytometer and microscope. Environ. Eng. Res. **24**: 397–403. doi:10.4491/eer.2018.266

Park, J., H. Lee, C. Y. Park, S. Hasan, T.-Y. Heo, and W. H. Lee. 2019b. Algal morphological identification in watersheds for drinking water supply using neural architecture search for convolutional neural network. Water **11**: 1338. doi:10.3390/w11071338

Parra, S. M., and others. 2020. Bonnet Carré Spillway freshwater transport and corresponding biochemical properties in the Mississippi bight. Cont. Shelf Res. **199**: 104114. doi:10.1016/j.csr.2020.104114

Patil, J. S., and A. C. Anil. 2015. Effect of monsoonal perturbations on the occurrence of phytoplankton blooms in a tropical bay. Mar. Ecol. Prog. Ser. **530**: 77–92. doi:10.3354/meps11289

Patil, J. S., R. V. Rodrigues, P. Paul, K. Sathish, M. Rafi, and A. C. Anil. 2017. Benthic dinoflagellate blooms in tropical intertidal rock pools: Elucidation of photoprotection mechanisms. Mar. Biol. **164**: 89. doi:10.1007/s00227-017-3123-z

Patil, J. S., and A. C. Anil. 2019. Assessment of phytoplankton photo-physiological status from a tropical monsoonal estuary. Ecol. Indic. **103**: 289–300. doi:10.1016/j.ecolind.2019.03.058

Pattullo, M. B., and others. 2019. Soil sealing by algae: An alternative to plastic pond liners for outdoor algal cultivation. Algal Res. **38**: 101414. doi:10.1016/j.algal.2019.101414

Plint, A. C., D. Moher, A. Morrison, K. Schulz, D. G. Altman, C. Hill, and I. Gaboury. 2006. Does the CONSORT checklist improve the quality of reports of randomised controlled trials? A systematic review. Med. J. Aust. **185**: 263–267. doi:10.5694/j.1326-5377.2006.tb00557.x

Plummer, S., A. E. Taylor, E. L. Harvey, C. M. Hansel, and J. M. Diaz. 2019. Dynamic regulation of extracellular superoxide production by the coccolithophore Emiliania huxleyi (CCMP 374). Front. Microbiol. **10**: 1546. doi:10.3389/fmicb.2019.01546

Poulin, R. X., S. Hogan, K. L. Poulson-Ellestad, E. Brown, F. M. Fernández, and J. Kubanek. 2018a. *Karenia brevis* allelopathy compromises the lipidome, membrane integrity, and photosynthesis of competitors. Sci. Rep. **8**: 1–9. doi:10.1038/s41598-018-27845-9

Poulin, R. X., K. L. Poulson-Ellestad, J. S. Roy, and J. Kubanek. 2018b. Variable allelopathy among phytoplankton reflected in red tide metabolome. Harmful Algae **71**: 50–56. doi:10.1016/j.hal.2017.12.002

Poulton, N. J. 2016. FlowCam: Quantification and classification of phytoplankton by imaging flow cytometry, p. 237–247. *In* Imaging flow cytometry. Springer.

Poulton, N. J., and J. L. Martin. 2010. Imaging flow cytometry for quantitative phytoplankton analysis - FlowCAM, p. 47–54. *In* B. Karlson, C. Cusack, and E. Bresnan [eds.], Microscopic and molecular methods for quantitative phytoplankton analysis. Intergovernmental Oceanographic Commission of UNESCO.

Pree, B., and others. 2017. Dampened copepod-mediated trophic cascades in a microzooplankton-dominated microbial food web: A mesocosm study. Limnol. Oceanogr. **62**: 1031–1044. doi:10.1002/lno.10483

Reul, A., E. Martín-Clemente, I. J. Melero-Jiménez, E. Bañares-España, A. Flores-Moya, and M. J. García-Sánchez. 2020. What triggers the annual cycle of cyanobacterium *Oscillatoria* sp. in an extreme environmental sulfide-rich spa? Water **12**: 883. doi:10.3390/w12030883

Reynolds, R., D. Stramski, V. Wright, and S. Woźniak. 2010. Measurements and characterization of particle size distributions in coastal waters. J. Geophys. Res. Oceans **115**: C08024. doi:10.1029/2009JC005930

Romero-Martínez, L., C. van Slooten, E. Nebot, A. Acevedo-Merino, and L. Peperzak. 2017. Assessment of imaging-in-flow system (FlowCAM) for systematic ballast water management. Sci. Total Environ. **603**: 550–561. doi:10.1016/j.scitotenv.2017.06.070

Roque, Y. S., Y. del Carmen Pérez-Luna, J. M. Acosta, N. F. Vázquez, R. B. Hernández, S. S. Trinidad, and J. S. Pathiyamattom. 2018. Evaluation of the population dynamics of microalgae isolated from the state of Chiapas, Mexico with respect to the nutritional quality of water. Biodivers. Data J. **6**: e28496. doi:10.3897/BDJ.6.e28496

Rue, G. P., J. P. Darling, E. Graham, M. M. Tfaily, and D. M. McKnight. 2020. Dynamic changes in dissolved organic matter composition in a Mountain Lake under ice cover and relationships to changes in nutrient cycling and phytoplankton community composition. Aquat. Sci. **82**: 1–16. doi:10.1007/s00027-019-0687-3

Rutten, T. P., B. Sandee, and A. R. Hofman. 2005. Phytoplankton monitoring by high performance flow cytometry: A successful approach? Cytometry A **64**: 16–26. doi:10.1002/cyto.a.20106

See, J. H., L. Campbell, T. L. Richardson, J. L. Pinckney, R. Shen, and N. L. Guinasso. 2005. Combining new technologies for determination of phytoplankton community structure in the Northern Gulf of Mexico 1. J. Phycol. **41**: 305–310. doi:10.1111/j.1529-8817.2005.04132.x

Segovia, M., and others. 2017. Iron availability modulates the effects of future $CO_2$ levels within the marine planktonic food web. Mar. Ecol. Prog. Ser. **565**: 17–33. doi:10.3354/meps12025

Segovia, M., M. R. Lorenzo, C. Iñiguez, and C. García-Gómez. 2018. Physiological stress response associated with elevated $CO_2$ and dissolved iron in a phytoplankton community dominated by the coccolithophore *Emiliania huxleyi*. Mar. Ecol. Prog. Ser. **586**: 73–89. doi:10.3354/meps12389

Selz, V., K. E. Lowry, K. M. Lewis, H. L. Joy-Warren, W. Van De Poll, S. Nirmel, A. Tong, and K. R. Arrigo. 2018. Distribution of *Phaeocystis Antarctica*-dominated sea ice algal communities and their potential to seed phytoplankton across the western Antarctic Peninsula in spring. Mar. Ecol. Prog. Ser. **586**: 91–112. doi:10.3354/meps12367

Sieracki, C. K., M. E. Sieracki, and C. S. Yentsch. 1998. An imaging-in-flow system for automated analysis of marine microplankton. Mar. Ecol. Prog. Ser. **168**: 285–296. doi:10.3354/meps168285

Sieracki, M. E., and others. 2010. Optical plankton imaging and analysis systems for ocean observation, p. 21–25. In J.

Hall, D. E. Harrison, and D. Stammer, [eds.], Proceedings of OceanObs'09: Sustained Ocean Observations and Information for Society *(Vol. 2)*. European Space Agency.

Smith, H. J., R. A. Foster, D. M. McKnight, J. T. Lisle, S. Littmann, M. M. Kuypers, and C. M. Foreman. 2017. Microbial formation of labile organic carbon in Antarctic glacial environments. Nat. Geosci. **10**: 356–359. doi:10.1038/ngeo2925

Soares, M., L. Lobão, L. Vidal, N. Noyma, N. Barros, S. Cardoso, and F. Roland. 2011. Light microscopy in aquatic ecology: Methods for plankton communities studies. Methods Mol. Biol. **689**: 215–227. doi:10.1007/978-1-60761-950-5_13

Solomon, C. M., M. Jackson, and P. M. Glibert. 2019. Chesapeake Bay's "forgotten" Anacostia River: Eutrophication and nutrient reduction measures. Environ. Monit. Assess. **191**: 265. doi:10.1007/s10661-019-7437-9

Spaulding, S. A., D. H. Jewson, R. J. Bixby, H. Nelson, and D. M. McKnight. 2012. Automated measurement of diatom size. Limnol. Oceanogr. Methods **10**: 882–890. doi:10.4319/lom.2012.10.882

Stamieszkin, K., N. J. Poulton, and A. J. Pershing. 2017. Zooplankton grazing and egestion shifts particle size distribution in natural communities. Mar. Ecol. Prog. Ser. **575**: 43–56. doi:10.3354/meps12212

Sun, X., and S. Sun. 2014. Automated marine plankton image techniques and its application. Adv. Earth Sci. **29**: 748–755. doi:10.11867/j.issn.1001-8166.2014.06.0748

Tian-Tian, L., H. Ping, L. Jia-Xing, K. Zhi-Xin, and T. Ye-Hui. 2019. Utilization of different dissolved organic phosphorus sources by *Symbiodinium voratum* in vitro. FEMS Microbiol. Ecol. **95**: fiz150. doi:10.1093/femsec/fiz150

Tran, K., and J. D. Ackerman. 2019. Mussels partition resources from natural waters under flowing conditions. Sci. Total Environ. **696**: 133870. doi:10.1016/j.scitotenv.2019.133870

Tseng, M., E. Yangel, and Y. L. Zhou. 2019a. Herbivory alters thermal responses of algae. J. Plankton Res. **41**: 641–649. doi:10.1093/plankt/fbz043

Tseng, M., J. R. Bernhardt, and A. E. Chila. 2019b. Species interactions mediate thermal evolution. Evol. Appl. **12**: 1463–1474. doi:10.1111/eva.12805

Turner, L., L. Shamseer, D. G. Altman, K. F. Schulz, and D. Moher. 2012. Does use of the CONSORT statement impact the completeness of reporting of randomised controlled trials published in medical journals? A Cochrane review. Syst. Rev. **1**: 60. doi:10.1186/2046-4053-1-60

Vaillancourt, R. D., C. W. Brown, R. R. Guillard, and W. M. Balch. 2004. Light backscattering properties of marine phytoplankton: Relationships to cell size, chemical composition and taxonomy. J. Plankton Res. **26**: 191–212. doi:10.1093/plankt/fbh012

Vandermeersch, G., and others. 2015. A critical view on microplastic quantification in aquatic organisms. Environ. Res. **143**: 46–55. doi:10.1016/j.envres.2015.07.016

Viana, T. V., and others. 2019. Massive blooms of *Chattonella subsalsa* Biecheler (Raphidophyceae) in a hypereutrophic, tropical estuary—Guanabara Bay, Brazil. Front. Mar. Sci. **6**: 85. doi:10.3389/fmars.2019.00085

Von Elm, E., D. G. Altman, M. Egger, S. J. Pocock, P. C. Gøtzsche, and J. P. Vandenbroucke. 2007. The Strengthening the Reporting of Observational Studies in Epidemiology (STROBE) statement: Guidelines for reporting observational studies. Ann. Intern. Med. **147**: 573–577. doi:10.1136/bmj.39335.541782.AD

Walcutt, N. L., and others. 2020. Assessment of holographic microscopy for quantifying marine particle size and concentration. Limnol. Oceanogr. Methods **18**: 516–530. doi:10.1002/lom3.10379

Wang, C., B. Feng, C. Tian, Y. Tian, D. Chen, X. Wu, G. Li, and B. Xiao. 2018a. Quantitative study on the survivability of Microcystis colonies in lake sediments. J. Appl. Phycol. **30**: 495–506. doi:10.1007/s10811-017-1246-8

Wang, C., Q. Cai, B. Feng, S. Feng, C. Tian, X. Jiang, X. Wu, and B. Xiao. 2019. Improving the performance of shipboard rotary drum filters in the removal of cyanobacterial blooms by cationic polyacrylamide flocculation. Sep. Purif. Technol. **215**: 660–669. doi:10.1016/j.seppur.2019.01.009

Wang, L., P. Liu, J. Sun, Y. Zhang, Q. Zhou, Z. Wu, and F. He. 2018b. Comparison and combination of selective grazing on natural seston by benthic bivalves (*Hyriopsis cumingii*) and pelagic fish (*Hypophthalmichthys molitrix*). Environ. Sci. Pollut. R. **25**: 33423–33431. doi:10.1007/s11356-018-3287-1

Wang, Y., M. Castillo-Keller, E. Eustance, and M. Sommerfeld. 2017. Early detection and quantification of zooplankton grazers in algal cultures by FlowCAM. Algal Res. **21**: 98–102. doi:10.1016/j.algal.2016.11.012

Wasmund, N., J. Kownacka, J. Göbel, A. Jaanus, M. Johansen, I. Jurgensone, S. Lehtinen, and M. Powilleit. 2017. The diatom/dinoflagellate index as an indicator of ecosystem changes in the Baltic Sea 1. Principle and handling instruction. Front. Mar. Sci. **4**: 22. doi:10.3389/fmars.2017.00022

Whalen, K. E., J. W. Becker, A. M. Schrecengost, Y. Gao, N. Giannetti, and E. L. Harvey. 2019. Bacterial alkylquinolone signaling contributes to structuring microbial communities in the ocean. Microbiome **7**: 93. doi:10.1186/s40168-019-0711-9

Wirth, C., R. Limberger, and T. Weisse. 2019. Temperature × light interaction and tolerance of high water temperature in the planktonic freshwater flagellates *Cryptomonas* (Cryptophyceae) and *Dinobryon* (Chrysophyceae). J. Phycol. **55**: 404–414. doi:10.1111/jpy.12826

Woods, M. N., M. E. Stack, D. M. Fields, S. D. Shaw, and P. A. Matrai. 2018. Microplastic fiber uptake, ingestion, and egestion rates in the blue mussel (*Mytilus edulis*). Mar. Pollut. Bull. **137**: 638–645. doi:10.1016/j.marpolbul.2018.10.061

Wu, H., T. Yang, C. Wang, C. Tian, O. O. Donde, B. Xiao, and X. Wu. 2020a. Co-regulatory role of *Microcystis* colony cell

volume and compactness in buoyancy during the growth stage. Environ. Sci. Pollut. Res. **27**: 42313–42323. doi:10.1007/s11356-020-08250-0

Wu, X., T. Yang, S. Feng, L. Li, B. Xiao, L. Song, A. Sukenik, and I. Ostrovsky. 2020b. Recovery of *Microcystis* surface scum following a mixing event: Insights from a tank experiment. Sci. Total Environ. **728**: 138727. doi:10.1016/j.scitotenv.2020.138727

Yang, Y., X. Sun, and Y. Zhao. 2017a. Effects of Lugol's iodine solution and formalin on cell volume of three bloom-forming dinoflagellates. Chin. J. Oceanol. Limnol. **35**: 858–866. doi:10.1007/s00343-017-5378-0

Yang, Y., X. Sun, M. Zhu, X. Luo, and S. Zheng. 2017b. Estimating the carbon biomass of marine net phytoplankton from abundance based on samples from China seas. Mar. Freshw. Res. **68**: 106–115. doi:10.1071/MF15298

Yokogawa Fluid Imaging Technologies. 2021. VisualSpreadsheet® Particle Analysis Software [accessed 2021 October 18]. Available from https://www.fluidimaging.com/products/particle-analysis-software-5

Yu, M. 2019. Preparation of polyelectrolyte-coated proteins for controlled drug delivery via supercritical fluid processing. PhD Thesis. Delft Univ. of Technology.

Zamyadi, A., K. E. Greenstein, C. M. Glover, C. Adams, E. Rosenfeldt, and E. C. Wert. 2020. Impact of hydrogen peroxide and copper sulfate on the delayed release of microcystin. Water **12**: 1105. doi:10.3390/w12041105

Zarauz, L., and X. Irigoien. 2008. Effects of Lugol's fixation on the size structure of natural nano–microplankton samples, analyzed by means of an automatic counting method. J. Plankton Res. **30**: 1297–1303. doi:10.1093/plankt/fbn084

Zhang, W., X. Sun, S. Zheng, M. Zhu, J. Liang, J. Du, and C. Yang. 2019. Plankton abundance, biovolume, and normalized biovolume size spectra in the northern slope of the South China Sea in autumn 2014 and summer 2015. Deep Sea Res. Pt. I **167**: 79–92. doi:10.1016/j.dsr2.2019.07.006

Zingone, A., P. J. Harrison, A. Kraberg, S. Lehtinen, A. McQuatters-Gollop, T. O'Brien, J. Sun, and H. H. Jakobsen. 2015. Increasing the quality, comparability and accessibility of phytoplankton species composition time-series data. Estuar. Coast. Shelf Sci. **162**: 151–160. doi:10.1016/j.ecss.2015.05.024

## Acknowledgments

This research has been supported by Murdoch University and the Department of Biodiversity, Conservation and Attractions (DBCA), project number SPP2018-029. The authors acknowledge the extensive advice and assistance provided by staff at DBCA, Department of Water and Environmental Regulation Phytoplankton Ecology Unit, Commonwealth Scientific and Industrial Research Organisation (CSIRO), Yokogawa Fluid Imaging Technologies and Kenelec Scientific. Access to the FlowCam used was provided by Muradel and some flow cells used were donated by Kenelec Scientific. Open access publishing facilitated by Murdoch University, as part of the Wiley - Murdoch University agreement via the Council of Australian University Librarians. Author contributions for this manuscript were as follows: B.O., C.H., J.C. and N.M. conceptualized the study. B.O. conducted the review and case studies and wrote the manuscript. C.H., J.C. and J.T. reviewed and edited drafts. J.C. and C.H. acquired funding. C.H., J.C., N.M and J.T. provided supervision to B.O. Open access publishing facilitated by Murdoch University, as part of the Wiley - Murdoch University agreement via the Council of Australian University Librarians.

*Submitted 01 November 2021*
*Revised 14 April 2022*
*Accepted 09 May 2022*

*Associate editor: Malinda Sutor*